Intersectional Impacts of the 2021 M_w 7.2 Nippes, Haiti, Earthquake from Geotechnical and Social Perspectives

Ashly Cabas[*1], Cristina Lorenzo-Velazquez[1], Nancy Ingabire Abayo[1], Chunyang Ji[1], Jenny Ramirez[2], Fernando E. Garcia[3], Joanne Pérodin[4], Yu-Wei Hwang[5], Shideh Dashti[6], Nazife Emel Ganapati[7], Sary Nicolas[8], Michael R. Z. Whitworth[9], Kelly Guerrier[10], Newdeskarl Saint Fleur[11], Santina Contreras[12], Richard Lagesse[13], Louis Herns Marcelin[14], and Christa L. Remington[15]

ABSTRACT

The M_w 7.2 Nippes, Haiti, earthquake occurred on 14 August 2021 in Haiti's southwest peninsula and in the midst of significant social, economic, and political crises. A hybrid reconnaissance mission (i.e., combined remote and field investigation) was coordinated to document damage to the built environment after the event. This article evaluates two ground-motion records available in Haiti in the context of the geology of the region and known areas with significant damage, such as Les Cayes. We also present a new map of time-averaged shear-wave velocity values to 30 m depth (V_{S30}) for Les Cayes and Port-au-Prince based on the geostatistical approach of kriging and accounting for region-specific geology proxies and field measurements of V_{S30}. Case studies of ground failure observations, including landslides and liquefaction triggering, are described as well as the intersection of social and engineering observations. Maps depicting this important intersection are provided to facilitate the assessment of how natural hazards and social conflicts have influenced the vulnerability of Haiti's population to earthquakes.

KEY POINTS

- The 2021 Nippes earthquake caused significant damage in the midst of social, economic, and political crises.
- A new geology-informed V_{S30} map is created, and intersections of social and engineering observations are presented.
- Multiple natural hazards and social conflicts influenced Haiti's vulnerability to the 2021 Nippes earthquake.

INTRODUCTION

Eleven years after the catastrophic 12 January 2010 M_w 7.0 earthquake located approximately 25 km from Haiti's capital, Port-au-Prince, the M_w 7.2 Nippes earthquake posed significant challenges for response and recovery in Haiti. The M_w 7.2 Nippes earthquake occurred at 08:29 a.m. local time on 14 August 2021, as a result of oblique faulting along the Enriquillo–Plantain Garden fault (EPGF) zone. The epicenter was located 10.6 km from the city of Petit-Trou-de-Nippes, 38.6 km from Les Cayes, and 75 km west of the epicenter corresponding to the 2010 M_w 7.0 Port-au-Prince earthquake (Dashti *et al.*, 2022). The dual hazards of this shallow earthquake (with focal depth of 10 km) and tropical storm grace two days afterward had a significant impact on the landscape and infrastructure of Haiti's southwestern peninsula, including structural damages, slope instability, landslides, ground

1. North Carolina State University, Raleigh, North California, U.S.A., https://orcid.org/0000-0002-1039-4053 (AC); https://orcid.org/0000-0003-1577-2874 (CL-V); https://orcid.org/0000-0002-9471-560X (CJ); 2. Geosyntec Consultants, Waterloo, Ontario, Canada; 3. Department of Civil and Environmental Engineering, University of Michigan, Ann Arbor, Michigan, U.S.A., https://orcid.org/0000-0001-7993-0347 (FEG); 4. Florida International University, Miami, Florida, U.S.A.; 5. National Yang Ming Chiao Tung University, Taiwan, Taipei City, Taiwan (Republic of China), https://orcid.org/0000-0002-2319-5336 (Y-WH); 6. University of Colorado Boulder, Boulder, Colorado, U.S.A.; 7. Department of Public Policy and Administration Steven J. Green School of International and Public Affairs, Florida International University, Miami, Florida, U.S.A., https://orcid.org/0000-0003-0967-9593 (NEG); 8. Langan Engineering, U.S.A.; 9. AECOM, Plymouth, United Kingdom, https://orcid.org/0000-0003-1837-3385 (MRZW); 10. URGéo-CARIBACT, Faculté des Sciences, Université d'État d'Haïti, Port-au-Prince, Haïti, https://orcid.org/0000-0002-1412-080X (KG); 11. Faculté des Sciences, Université d'Etat d'Haïti, LMI CARIBACT, Urgéo, Port-au-Prince, Haïti; 12. University of Southern California, Los Angeles, California, U.S.A., https://orcid.org/0000-0003-4461-607X (SC); 13. ARUP, London, United Kingdom, https://orcid.org/0000-0001-7843-5045 (RL); 14. University of Miami, Miami, Florida, U.S.A., https://orcid.org/0000-0002-9238-9695 (LHM); 15. University of South Florida, Zephyrhills, Florida, U.S.A., https://orcid.org/0000-0001-8979-4545 (CLR)

*Corresponding author: amcabasm@ncsu.edu

Cite this article as Cabas, A., C. Lorenzo-Velazquez, N. Ingabire Abayo, C. Ji, J. Ramirez, F. E. Garcia, J. Pérodin, Y.-W. Hwang, S. Dashti, N. E. Ganapati, *et al.* (2023). Intersectional Impacts of the 2021 M_w 7.2 Nippes, Haiti, Earthquake from Geotechnical and Social Perspectives, *Bull. Seismol. Soc. Am.* **XX**, 1–26, doi: 10.1785/0120220118

failures, and strong ground shaking. In addition, response efforts faced challenges due to the COVID-19 pandemic and ongoing political instability in the country. These cascading events highlighted the need for short-term response and long-term recovery strategies to work within the greater social–political–cultural context of Haiti. The aim of this article is to examine the 2021 M_w 7.2 Nippes, Haiti, earthquake through the lenses of ground motions, geohazards, and social impacts. In pursuit of that goal, we build upon the interdisciplinary Geotechnical Extreme Events Reconnaissance (GEER) team's efforts to further investigate relevant case studies after this event, and describe meaningful intersections between engineering observations and social sciences.

In this study, we first summarize our hybrid reconnaissance activities (i.e., combined remote and field investigation). Then, we describe the characteristics of the ground-motion records available from the mainshock, and the development of a new map of time-averaged shear-wave velocity values to 30 m depth (V_{S30}) for Les Cayes and Port-au-Prince based on the geostatistical approach of kriging and accounting for region-specific geologic proxies and field measurements of V_{S30}. Single-station analyses to investigate potential site effects in regions of interest are also evaluated, and two specific geotechnical engineering hazards from the 2021 Nippes earthquake are analyzed as part of case studies on landslides and liquefaction-induced ground failure. Finally, we explore the intersection of different crises in Haiti since 2010, along with the social–political–economic effects of these crises.

RECONNAISSANCE ACTIVITIES

The remote reconnaissance team consisted of experts in geotechnical earthquake engineering, engineering geology and seismology, engineering geomorphology, and social and political implications of disasters. Because of the nature of this event and lack of immediate physical presence of the team (due to safety and security concerns), we initially collected perishable data and information from a variety of sources (from satellite imagery to social media). The details of our data collection approach are provided in Dashti *et al.* (2022).

In parallel to engineering reconnaissance, social science data collection was designed based on team members' prior research in Haiti and a review of secondary sources described herein. After the 2010 Haiti earthquake, some team members conducted research on shelter recovery, social capital, public participation, and work-related challenges faced by those involved in disaster response and recovery (e.g., emotional challenges and cultural competencies). The work was based on interviews, surveys, focus groups, and Town Hall meetings with various stakeholders (see Remington and Ganapati, 2017; Contreras, 2019; Ganapati and Mukherji, 2019; Kroll *et al.*, 2021 for details on methods). Secondary data sources, focusing on the effects of the 2021 Nippes earthquake in Haiti, were mainly: (1) Haitian government agencies (e.g., Ministry of Public Health [Ministère de la Santé Publique et de la Population]); (2) Haitian (e.g., Quisqueya University [Université Quisqueya]) and international universities, think tanks, and research institutes (e.g., Pew Research Center); (3) Haitian (e.g., Le Nouvelliste) and international news sources (e.g., Reuters); (4) international aid agencies (e.g., the World Bank, the United Nations [UN] Development Program, UN Office for Coordination of Humanitarian Assistance, UN International Organization for Migration, and UN Security Council); and (5) disaster-focused databases (e.g., EM-DAT International Disaster Database).

GEOTECHNICAL SIGNIFICANCE AND INTERSECTION WITH SOCIAL FACTORS

About 96% of Haiti's population are vulnerable to natural hazards (World Bank, 2021). The 2021 M_w 7.2 Nippes earthquake occurred in conjunction with significant social, economic, and political crises as well as with other hazards, such as Tropical Storm Grace and the COVID19 pandemic. The complex spatiotemporal interactions among natural hazards, and socioeconomic and political crises made the population especially vulnerable to the aftermath of the 2021 earthquake. In this study, we examine how multiple crises in the recent history contribute to Haiti's vulnerability to natural hazards. Figure 1 outlines different crises in Haiti since 2010 and their effects on population displacement. Understanding people displacement patterns to areas with high seismic hazards and/or significant geohazards can improve future recovery and resilience practices in Haiti. For instance, the 2010 Port-au-Prince earthquake and Hurricane Matthew in 2016 have caused the most significant population displacements to date.

The challenges that characterize Haiti as a fragile state have amplified in recent years. Natural hazards and social conflicts have influenced the population's vulnerability to earthquake-induced failure of infrastructure, such as that induced by ground failure and/or structural collapse. Nearly 33,000 victims of the 2010 earthquake still live in displacement camps, and over 300,000 have not received government assistance to resettle (Internal Displacement Monitoring Centre [IDMC], 2020). In addition, over 140,000 families displaced by Hurricane Matthew in 2016 (Fig. 1) have not secured a decent shelter to date (IDMC, 2021). According to the Human Rights Watch (2020), from January to August 2020, an estimated 944 intentional homicides, 124 kidnappings, and 159 deaths resulting from gang violence have been reported by the United Nations Integrated Office in Haiti (BINUH). At least 12,000 displacements that same year are attributed to gang violence and Hurricane Isaias (ReliefWeb, 2021). The IDMC, established in 1998 as part of the Norwegian Refugee Council (NRC), reported an estimated 2.03 million new displacements linked to disasters in Haiti from 2008 to 2020 (IDMC, 2021). Further, the population density has increased since 2008, particularly in Les Cayes, Petit-Goave, Grand-Goave, and Leogane locations where there was concentrated damage after the 2021 Haiti earthquake

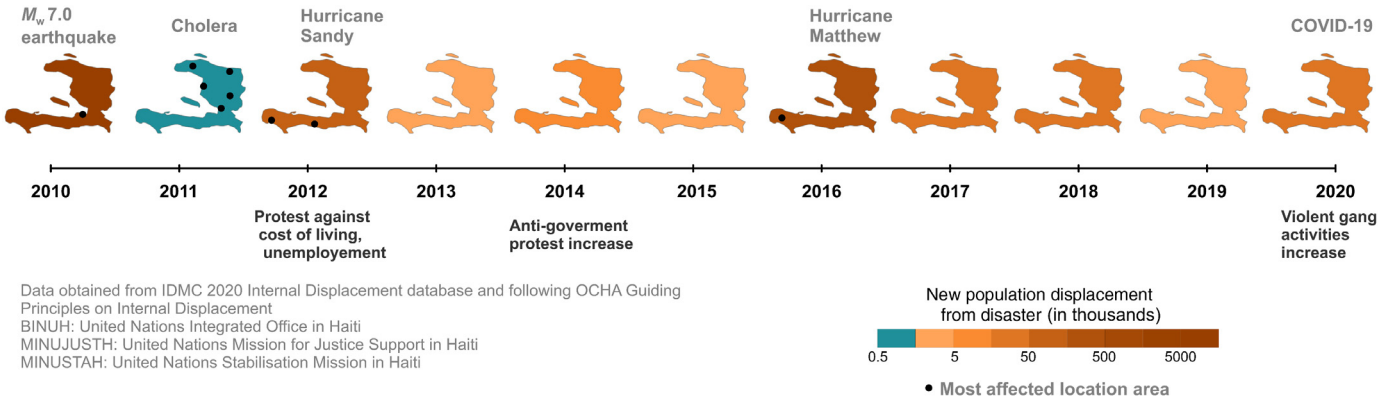

Figure 1. Sociopolitical crises and natural disasters in Haiti since 2010, including the corresponding new population displacements from each event (sources noted in the legend). The color version of this figure is available only in the electronic edition.

(see Fig. 2). The aforementioned cities are also located on Quaternary surficial deposits, which can amplify the amplitude of seismic waves and increase the duration of earthquake ground shaking. This means that population displacements due to the previous disasters in the region resulted in more people living in areas of potentially higher seismic hazard. The IDMC (2020) also reported an estimated 10,000 new displacements from conflict in 2019 and 2020 (Fig. 1). Since April 2022, a new wave of violence has led to the internal displacement of an estimated 17,000 people, from the Port-au-Prince metropolitan area to other areas in the country (International Organization for Migration [IOM], 2022). These displacements also influence the population's vulnerability to seismic hazards and related geohazards, such as landslides and liquefaction-induced ground deformation. Moreover, concurrent crises (as well as the cumulative effects of multiple and frequent crises on the social fabric) hinder the deployment of traditional postdisaster reconnaissance missions, limiting the collection of relevant perishable data, challenging the acquisition of new knowledge to improve the performance of civil infrastructure in future extreme events, and jeopardizing resilience planning for the communities that need it the most.

The 2021 Nippes seismic event caused widespread landslides throughout Haiti's southwestern peninsula, particularly along National Route 7 (RN7; Dashti *et al.*, 2022). The latter serves the communes of Les Cayes, Camp-Perrin, Roseaux, Beaumont, and Jérémie. Before this earthquake, and following that of 2010, the southern region of Haiti had been hit by over 20 disasters—flooding, drought, epidemic, hurricanes—contributing to an estimated 7800 lives lost and over two billion dollars in total damages (EM-DAT, 2021). Significant landslide activity was observed following the 2021 earthquake in steep, mountainous terrain, particularly in Pic Macaya National Park (Garcia *et al.*, 2022). Landslide and rockfall debris created road blockages and caused significant damage to pavement and retaining walls along RN7, while evidence of liquefaction was found along the main trace of the EPGF zone. These ground failures imposed significant stress to lifelines in the region, hindering the distribution of basic goods, aid efforts, and travel to and from affected areas. In addition, considering the geology and seismicity in Haiti, as well as the documented contribution of local soil conditions on the observed damage after the 2010 Port au Prince earthquake (known as site effects; Rathje *et al.*, 2010), there is a need to further understand potential site effects after this event. Stronger ground shaking due to site effects in certain areas may explain observed damage patterns in some of the most affected areas, and could provide necessary evidence for future improvements of building codes and urban resiliency plans.

Notably, among the most relevant differences between the 2010 and 2021 events in Haiti, the availability of records from the 2021 event, which allows for the investigation of ground-motion characteristics in the region (Cabas *et al.*, 2022) and potential site effects. Citizen science efforts in Haiti (Calais *et al.*, 2022) enabled the operation of low-cost seismometers that ultimately provided data on aftershocks and the closest record to the epicenter of the 2021 mainshock. The previous studies in the region have shown that active community engagement in earthquake science might effectively contribute to reducing seismic risk by collecting scientifically relevant seismological data and increasing earthquake awareness (Calais *et al.*, 2020).

GEOLOGY OF AFFECTED REGIONS WITHIN HAITI

The Nippes 2021 earthquake devastated various regions within the southern peninsula of Haiti, especially within the mountain range of La Hotte (see Data and Resources). An understanding of the geology of affected regions after seismic events is essential to evaluate geohazards and observed damages. Hence, our study focuses on areas where significant damage was observed and provides a description of the relevant geologic units.

A remarkable length of the coast of the Massif de la Hotte consists of reef limestones, with a 3–4 km extent in width. Limestones (Tml) and other carbonate deposits (e.g., Tca, Tmcc, Kcr, and QTcr) dominate this region, as shown in Figure 2.

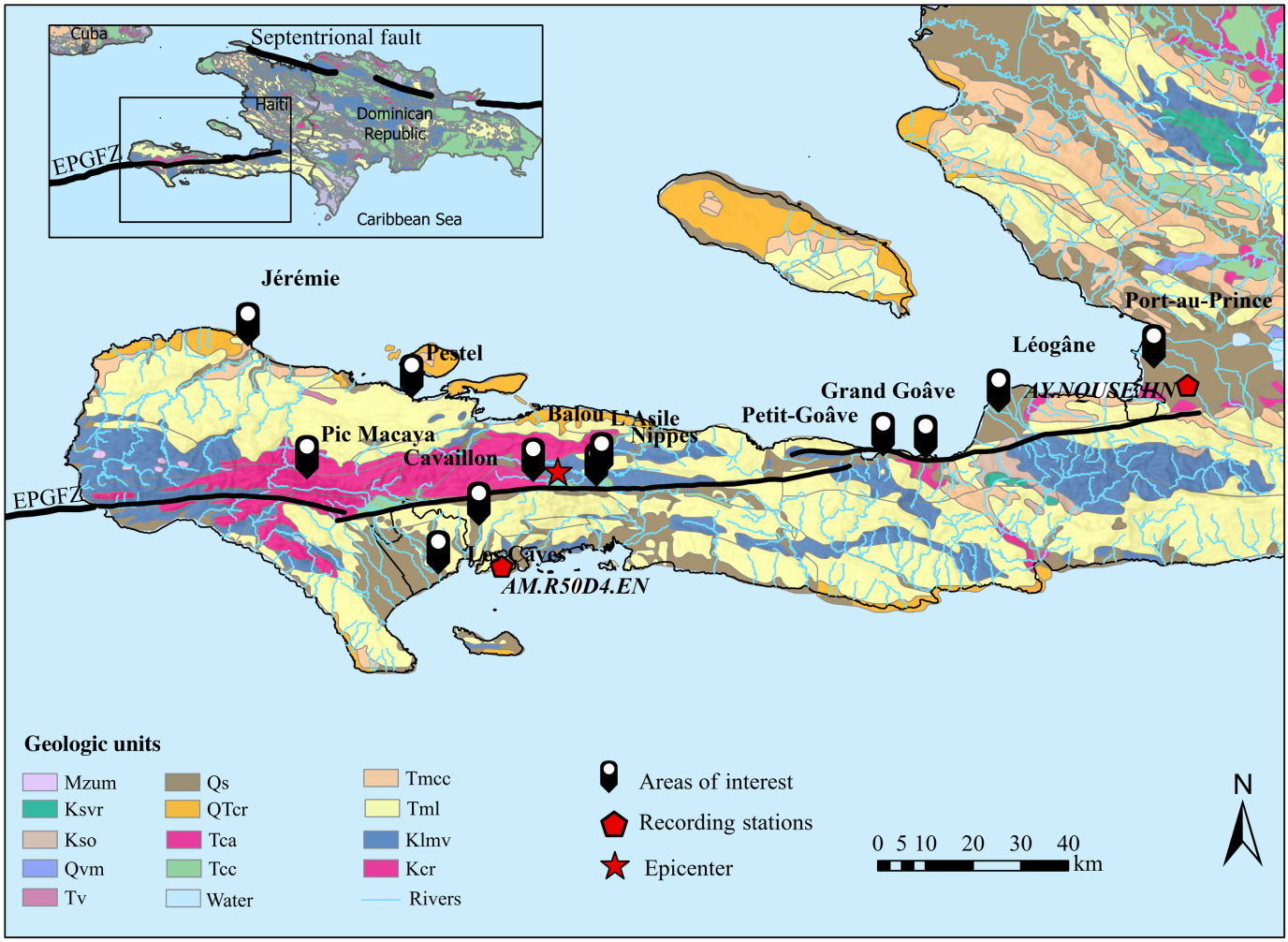

Rivière de Grand Anse (which flows through Jérémie) is the largest river in the southern peninsula of Haiti. Within the valleys of the rivers and coastal plains, especially the region of Les Cayes, the quaternary alluvial formations dominate (Butterlin, 1960). These include lithified and loose sediments that coincide with the Quaternary surficial deposits (Qs) (Butterlin, 1960; French and Schenk, 2004).

The bedrock geology in the region of Les Cayes includes various conglomerates, shales, and limestones, typically white–yellow chalky limestones (Butterlin, 1960), which dominate the northern part. Les Cayes hosts four main rivers or streams: Ravine du sud, Rivière de l'Islet, Rivière de Torbeck, and Rivière de l'Acul (Dashti *et al.*, 2022). These fluvial systems contribute to the deposition of the quaternary alluvial soils, which are likely susceptible to liquefaction and consistent with observations of sand boils (Dashti *et al.*, 2022). Based on limited borehole data, the top 15–30 m are characterized by a mixture of gravel, silty and clay sand, sandy silts, and sandy clays. Furthermore, this region is also characterized by the abundance of both surface and groundwater resources (Dashti *et al.*, 2022).

Figure 2 shows the location of the regions that were mostly affected by the Nippes 2021 earthquake, including Les Cayes, Jeremie, Pestel, Pic Macaya, Caviallon, L'Asile, Balou, and Nippes. Carbonate deposits are more abundant in Jeremie than in Les Cayes. In contrast, Jeremie has less alluvial deposits than Les Cayes. The alluvial deposits near Jeremie are mostly in the vicinity of Rivière Grand'Anse, Rivière La Voldrogue, and Rivière Guinaudée. Pestel is characterized by mostly limestone (with some chert) geologic units as well as some alluvial deposits in the vicinity of Rivière Glace. Pic Macaya is characterized by elevated topography, and lies within limestone and chert (Kcr) deposits (Butterlin, 1960; French and Schenk, 2004; Wilson *et al.*, 2019). Cavaillon also lies within some limestone (Tml) deposits, limestone and chert (Kcr), as well as some quaternary alluvial deposits in the proximity of Rivière De

Figure 2. Regional geological map with locations where ground failure or damage was observed (modified after Wilson *et al.*, 2019). The Septentrional fault (to the north) and the Enriquillo Plantain Garden fault zone (EPGFZ) are also shown (after Styron *et al.*, 2018). The locations of the 2021 Nippes earthquake epicenter (star) and two ground-motion recording stations (pentagons) are also shown. The inset figure shows the state level administrative boundaries of Haiti, Dominican Republic, and Cuba as well as two of the major active faults in the region. The color version of this figure is available only in the electronic edition.

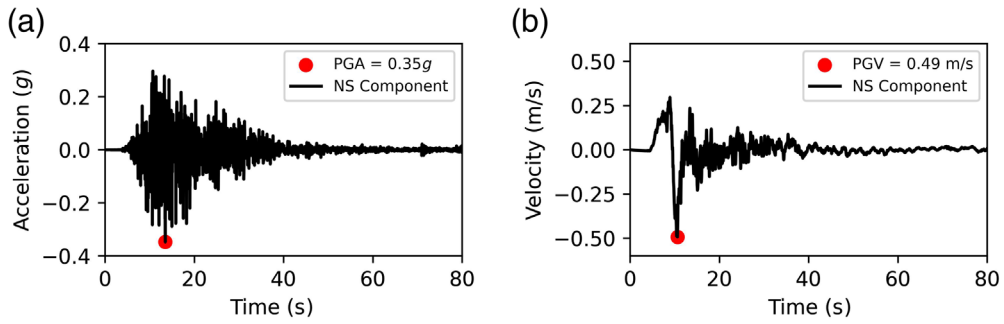

Figure 3. (a) Acceleration and (b) velocity time series at station AM.R50D4 corresponding to the NS horizontal component. The color version of this figure is available only in the electronic edition.

Cavaillon and Rivière De Boulmier. L'Asile and Balou are both located in the greater department of Nippes, which comprises Late-Cretaceous basalt, breccia, and tuff deposits (Klmv), continental clastic rocks (Pliocene to miocene, Tcc), some alluvial deposits near Rivière Dose and Rivière Mahot, as well as some deposits associated with carbonate reefs and reef complexes (QTcr). The damages observed in these regions are described in the Ground failure observations sections of this article.

GROUND-MOTION CHARACTERISTICS

Tectonic setting

Haiti is geologically and tectonically relatively young, and is in a complex, dynamic, and unstable tectonic regime that has developed in the last 12–15 million years. The North America, South America, Nazca, and Cocos plates are located in the perimeter of the Caribbean plate, and their relative motion characterizes complex and diverse tectonic regimes in the region (see Data and Resources). However, Haiti remained seismically quiescent during the 20th century, prior to the 12 January 2010 Port-au-Prince earthquake (Eberhard *et al.*, 2010).

Hispaniola is situated on a complex plate boundary where the predominant tectonic motions are left-lateral strike-slip between the North America and Caribbean plates, but there are also two converging subducting slabs beneath the Greater Antilles crust, where Hispaniola is situated. Over time, the tectonic motions have imparted a series of major left-lateral strike-slip faults, including the Septentrional fault in the north and the EPGF in the south (where the 14 August 2021 Nippes, Haiti, earthquake took place). Further details about the tectonic setting of Haiti are provided in Dashti *et al.* (2022).

Observed ground motions

After the 2010 Port-au-Prince seismic event, the Geological Survey of Canada (GSC) along with the U.S. Geological Survey (USGS) and Géoazur installed seismographs and strong-motion stations in Haiti (Bent *et al.*, 2018). Three GSC stations consisting of collocated weak- and strong-motion instruments comprised the first real-time seismic network in Haiti, which were used to monitor aftershocks (Bent *et al.*, 2018). Haiti also established its own network consisting of two seismographs and five accelerograph stations with real-time data availability and three additional nonreal-time strong-motion stations (Bent *et al.*, 2018; Calais *et al.*, 2020). In 2019, a community-seismology project (i.e., Ayiti-SEISMES) deployed low-cost Raspberry Shake sensors. Real-time regional data from USGS stations located in Cuba, Jamaica, the Dominican Republic, and the Turks and Caicos as well as stations from the Dominican Republic seismograph network provide supplemental seismic information for the region (Bent *et al.*, 2018).

Only ground motion records from the mainshock with epicentral distances less than 250 km are processed in this study using the USGS gmprocess software (Hearne *et al.*, 2019), which can automatically retrieve, download, and process ground motions for given earthquake events from major data providers (e.g., Incorporated Research Institutions for Seismology Data Management Center [IRIS-DMC]). The baselines were corrected, and a fifth-order Butterworth high- and low-pass filter was applied. The low-pass corner frequency was determined based on signal-to-noise ratios larger than 3.0 over a preselected frequency range. The high-pass corner frequency was selected following the algorithm of Ramos-Sepúlveda *et al.* (2022), which includes constraints to displacement values by (1) limiting the absolute displacement at the end of the time series (Dawood *et al.*, 2016) and (2) limiting the maximum amplitude of a third-order polynomial fit to the displacement time series. This recently proposed selection process for high-pass corner frequencies results in improved quality of long-period motion.

Four stations in Haiti, Dominican Republic, and Cuba recorded ground motions from the 2021 Nippes earthquake (Dashti *et al.*, 2022). As shown in Figure 2, only two stations are located in Haiti, namely a Raspberry Shake sensor (AM.R50D4 with latitude of 18.23° and longitude of −72.25°) and the U.S. Embassy strong-motion station (AY.NQUSE with latitude of 18.56° and longitude of −73.61°). The acceleration and velocity time series corresponding to the north–south horizontal component of the recorded ground motion at AM.R50D4 are provided in Figure 3. A velocity pulse indicative of potential directivity effects is identified in Figure 3b. The epicentral distance corresponding to this record is 24.9 km, which may be considered near-source, and the EPGF (a strike-slip fault) trace trends approximately east–west, and the velocity pulse only becomes apparent in the fault-normal orientation. However, the

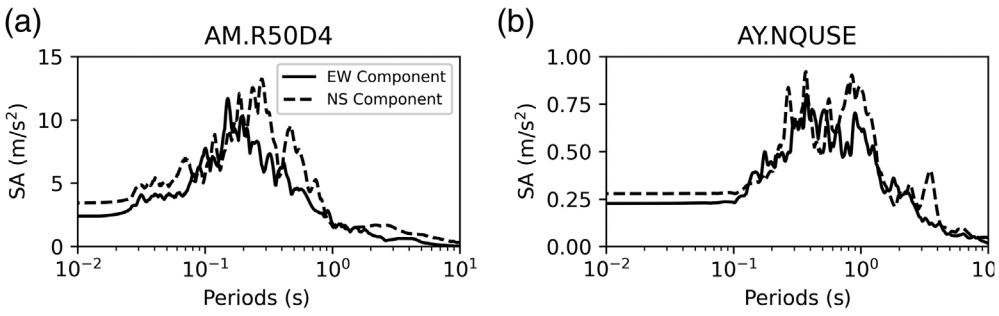

Figure 4. 5%-damped response spectra of records at (a) AM.R50D4 and (b) AY.NQUSE.

PGV does not reach a particularly large value (<100 cm/s). Hence, more research is needed to confirm the source of the observed velocity pulse.

Response spectra (5% damped) corresponding to the two orthogonal horizontal components recorded at AM.R50D4 and AY.NQUSE are provided in Figure 4. Ground-motion polarization is observed at both the stations (more significantly at AM.R50D4) and could be explained by anisotropy of the local soil conditions (Ramos-Sepúlveda and Cabas 2021). The amplification of long-period motion only present in the north–south component of the ground motion from AM.R50D4 may also indicate potential directivity effects. Predominant periods (i.e., the periods corresponding to the maximum amplitudes) for the NS component at AM.R50D4 and AY.NQUSE are 0.28 and 0.37 s, respectively. The significant duration and other common ground-motion intensity measures corresponding to these recorded motions from the mainshock are provided in the corresponding GEER report (Dashti *et al.*, 2022).

Subsurface characterization in Les Cayes and Port au Prince

The subsurface conditions at the two seismic stations that recorded the mainshock (i.e., AM.R50D4 and AY.NQUSE) were unknown by the time of completion of this study. Hence, we focused on advancing the characterization of near-surface geologic structures within areas that (1) experienced significant damage after the 2021 Nippes earthquake and (2) where measurements of the time-averaged shear-wave velocity in the top 30 m (V_{S30}) were available. Unfortunately, among the main affected locations in this event, Les Cayes was the only region that complies with our criteria (i.e., observed damage and availability of V_{S30} data).

A regional map that integrates geologic-based V_{S30} and measured V_{S30} is generated for Les Cayes using various geostatistical techniques and data from the whole country. Following similar efforts in California, Central and Eastern U.S., and Texas (e.g., Wills and Clahan, 2006; Thompson *et al.*, 2014; Parker *et al.*, 2017; Zalachoris *et al.*, 2017) measured V_{S30} from Les Cayes, and other regions in Haiti were matched to geologic units based on their geographic location. Available measured values represented three main regions, with most of the data coming from Port-au-Prince, followed by the region of Les Cayes (found on the southern west side of the country, see Fig. 2), Ganthier, and select data points from Cap-Haitien (both found on the southern west end of the country, see Fig. 2). A total of 280 measured V_{S30} values are included in our database and were obtained from Cox *et al.* (2011) and GeoTechMap (see Data and Resources) using multichannel analysis of surface waves (MASW) methods. A histogram depicting the distribution of V_{S30} values in our database is presented in Figure 5. Other types of geotechnical data were available within the areas of interest, such as six standard penetration tests (SPTs), several PANDA (Pénétromètre dynamique léger à énergie variable) measurements, dynamic penetration super Heavy measurements, and well logs. However, several of these measurements did not reach a depth of 30 meters. For example, only two of these SPTs reached the depth of 30 m, which resulted in only measured V_{S30} values from MASW tests being used in this study.

The pairing of measured V_{S30} values and geologic units presented in Table 1 was conducted by referencing the geologic map (scale 1:500,000) of the Great Antilles compiled by Wilson *et al.* (2019), and, where possible, the geologic map (scale 1:250,000) by Butterlin (1960) obtained through the Bureau des Mines et de l'énergie d'Haïti (see Data and Resources) was also consulted. There are eight groups that are based on both the geologic age and the lithologic unit (Table 1); coincidentally, each lithology has a different age based on the available geologic map. The geologic conditions in Les Cayes and Port-au-Prince are depicted in more detail in Figure 6 for comparison purposes. Thirty-eight percent of the measured V_{S30} values correspond to Quaternary surficial deposits that are undifferentiated. Approximately 2% correspond to the boundary between Quaternary and Upper Tertiary (Pliocene), and the recorded lithology is classified as deposits associated with carbonate reefs and reef complexes. Twenty-six percent of the measured values represent Calcarenite, biocalcarenite, limestone, and marl from the Pliocene (Tertiary) to Miocene epochs. One V_{S30} value was measured from Continental clastic rocks from the Pliocene to Mioceone epochs as well. Nearly 8% of the measured values were found within the mixed clastic and carbonate rocks corresponding to the Tertiary to the Miocene epochs. Twenty percent of the values were recorded in Limestone from the middle Miocene to the middle Eocene epochs. There were also Basalt, pillowed and nonpillowed flows, breccia, and tuff deposits from the Late Cretaceous,

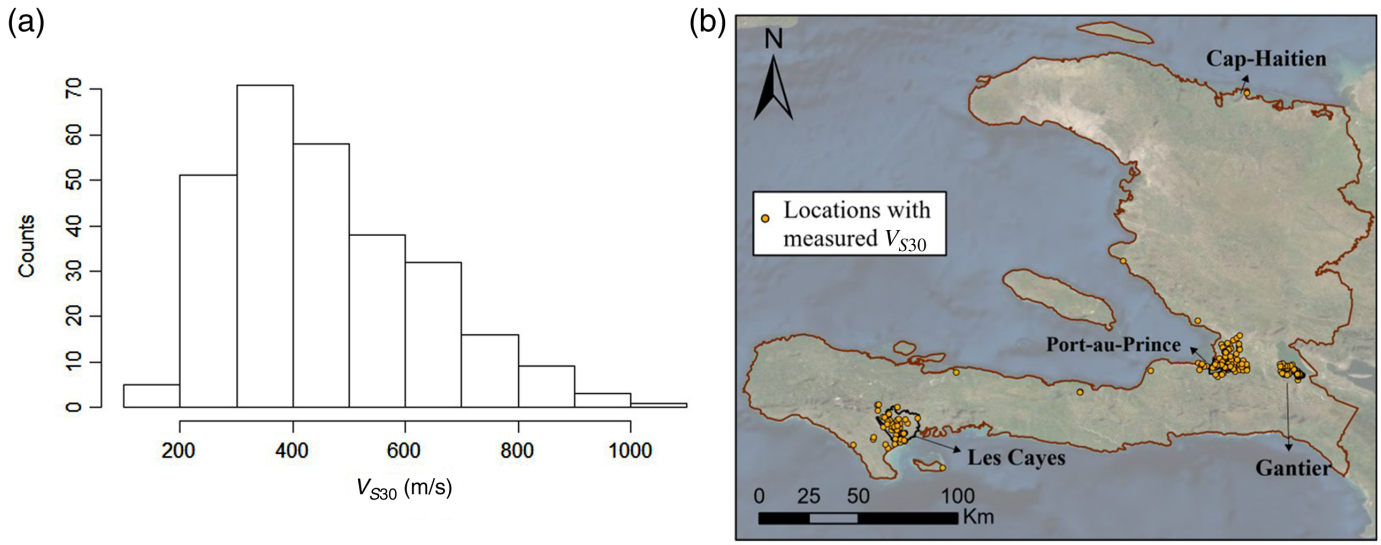

Figure 5. (a) Spatial distribution of the 280 measured V_{S30} values used in this study (depicted by yellow circles) and (b) its corresponding histogram of available V_S data in this study. The color version of this figure is available only in the electronic edition.

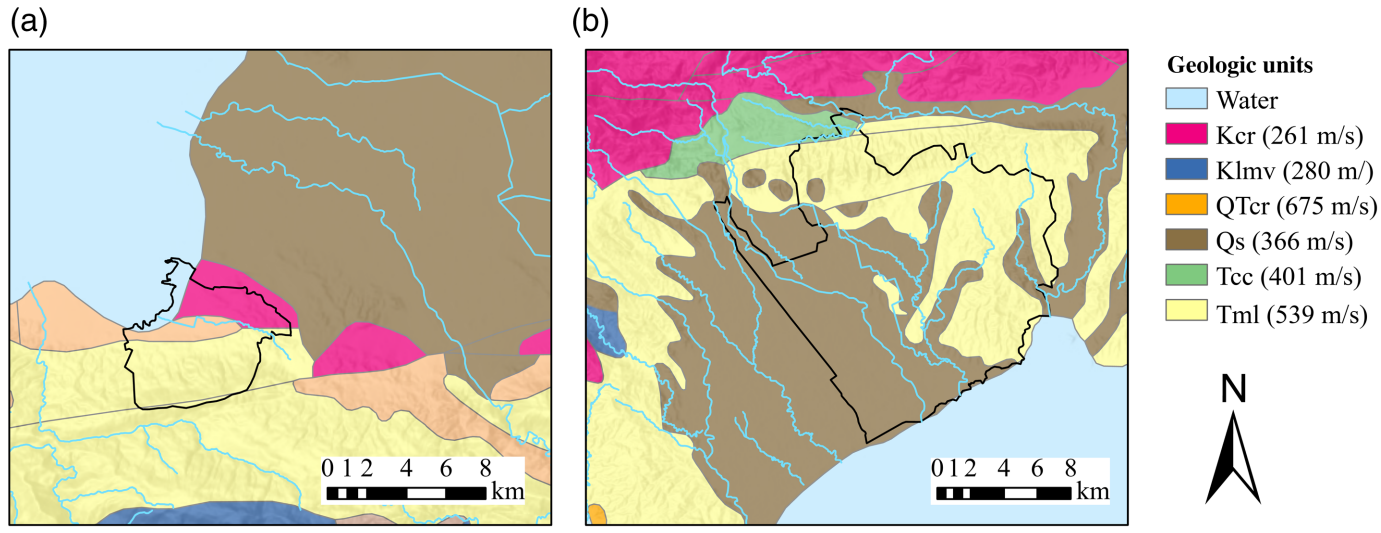

Figure 6. Geologic conditions within (a) Port-au-Prince and (b) Les Cayes along with the geology-informed V_S30 values assigned to each unit based on Table 1. The color version of this figure is available only in the electronic edition.

Maastrichtian to Santonian stages, which account for 5% of the measured V_{S30}. Finally, two of the measured values were also from the Cretaceous period, but corresponded to limestone and chert deposits. A set of four of the measured values plot outside of any area mapped as a geologic unit, which was an issue also found in Wills and Clahan (2006) study. These values plot within water bodies based on the geologic map that was employed in this study. However, based on the world topographic map from ESRI, these locations are on land, which is why they were excluded from the study. Furthermore, based on the maps by Butterlin (1960) and French and Schenk (2004), some of these points also correspond to different geologic units. In cases where these sources were not in agreement, the corresponding points were discarded to minimize potential bias.

The average V_{S30} for each geologic unit was obtained along with the standard deviation, assuming a log-normal distribution following Wills and Clahan (2006) and Parker *et al.* (2017) (see Table 1). When the sample size allowed for a normality check, this assumption was verified. For smaller sample sizes (i.e., for Tcc and Kcr), the arithmetic average of available V_{S30} values in those groups was used instead. Moreover, the maximum standard deviation measured among all geologic units was assumed

TABLE 1
Geologic Units and Shear-Wave Velocity Characteristics for Haiti Assuming a Log Normal Distribution for the Majority of the Geologic Units

Geologic Unit	Geologic Description	Number of Profiles	$\mu_{\ln VS30}$ (m/s)	$\sigma_{\ln VS30}$
Qs	Quaternary—surficial deposits, undifferentiated	107	366	1.61
QTcr	Quaternary and Upper Tertiary (Pliocene)—deposits associated with carbonate reefs and reef complexes	5	675	1.36
Tca	Pliocene (Tertiary) to Miocene—calcarenite, biocalcarenite, limestone, and marl	74	455	1.37
Tcc*	Pliocene to Mioceone—continental clastic rocks	1	401	1.61
Tmcc	Tertiary to the Miocene—mixed clastic and carbonate rocks	21	435	1.46
Tml	Tertiary Middle Miocene to the Middle Eocene—Limestone	57	539	1.29
Klmv	Late Cretaceous, Maastrichtian to Santonian—basalt, pillowed and nonpillowed flows, breccia, and tuff	13	280	1.23
Kcr*	Cretaceous period—Limestone and chert	2	261	1.61

*The arithmetic means and the maximum standard deviation were used (data were obtained from GeoTech Map).

for Tcc an Kcr as shown in Table 1. Because of limited information about the geologic classification (i.e, a wide range of composition covering a large geologic period per unit), there was not enough similarity in composition and geologic age to confidently borrow standard deviations from other geologic units (e.g., following Li *et al.*, 2022). As a result, assigning the maximum standard deviation obtained from the measured data (i.e., a $\sigma_{\ln VS30}$ of 1.61 m/s) corresponding to other geologic units to those with scarce data was deemed a more reasonable and conservative assumption. The quaternary surficial deposits in this study have a geology-based average V_{S30} (i.e., $\mu_{\ln VS30}$ in Table 1) that is within the reported range for Quaternary alluvium deposits by similar studies (e.g., Parker *et al.*, 2017 [209–448 m/s]; Thompson *et al.*, 2014 [145–649 m/s]; Wills and Clahan, 2006 [155–438 m/s]; Zalachoris *et al.*, 2017 [363–512 m/s]; and Li *et al.*, 2022 [210–436 m/s]). The geology-informed V_{S30} map was compared with the topographic slope-based proxy map for this study.

After determining the geology-informed V_{S30} values shown in Table 1, the available measured V_{S30} values were incorporated into a geostatistical approach to capture the spatial variation of this site term in Les Cayes and Port-au-Prince. We provide the spatial variability of V_{S30} in Port-au-Prince because of the high concentration of measured V_{S30} in that area and its significance, as evidenced by damages documented in the 2010 Haiti earthquake. In this study, we use kriging—a geostatistical interpolation approach that quantifies the spatial correlation structure of the data and determines the predicted values for locations with no observations or measurements within the study area. This method can be described as follows (Goovaerts, 1997):

$$Z(u_j)-\mu(u_j)=\sum_{i=1}^{n}\lambda_i(u_j)[Z(u_i)-\mu(u_i)], \tag{1}$$

in which $Z(u_i)$ is the value at sampled locations (u_i), $Z(u_j)$ is the interpolated value at unsampled locations (u_j), $\lambda_i(u_j)$ is the weight assigned at each location with the n measurements of $Z(u_i)$, and the mean value of Z at sampled and unsampled locations are $\mu(u_i)$ and $\mu(u_i)$, respectively. In this study, we followed this general approach by implementing kriging with an external drift, as described by Thompson *et al.* (2014) and Li *et al.* (2022) Kriging with an external drift varies from kriging with a trend (in which $\mu(u_j)$ depends on its spatial location); as the former performs the regression for the trend separately of the interpolation and subsequently, it is fitted to the trend's residual (Thompson *et al.*, 2014). For the interpolation simple kriging (SK) is applied, as it assumes $\mu(u_j)$ is a known constant as opposed to ordinary kriging, which assumes $\mu(u_j)$ is an unknown constant. In this, study we have defined the V_{s30}^{geol} as our known constant. First, the normalized residuals (r_n) assuming a log-normal distribution (e.g., Foster *et al.*, 2019) at each location with a measured V_{S30} (V_{s30}^{obs}) value were calculated to account for the V_{S30} estimated from geologic data (V_{s30}^{geol}, $\mu_{\ln VS30}$ in Table 1) as follows:

$$r_n=\frac{(V_{s30}^{\text{obs}})-\ln(V_{s30}^{\text{geol}})}{\sigma_{\ln(V_{s30})}^{\text{geol}}}, \tag{2}$$

in which $\sigma_{\ln(V_{s30})}^{\text{geol}}$ is the standard deviation of $\ln(V_{S30})$ based on geology. Then SK was performed on those normalized residuals, and the interpolated normalized residuals (r_i) at an unsampled location is the weighted summation of the normalized residuals at the sampled locations. To obtain the r_i at unsampled locations, a grid within the area with spacings of 500 m was generated for Haiti, and the V_{S30}geologic proxy was assigned at each location. Based on Thompson *et al.* (2014), the Whittle–Mátern semivariogram model is used to fit the data, which is given by

$$\gamma(h)=\sigma^2\left[1-\frac{2^{1-\nu}}{\Gamma(\nu)}\left(\frac{h}{a}\right)^{\nu}K_{\nu}\left(\frac{h}{a}\right)\right]+\tau, \tag{3}$$

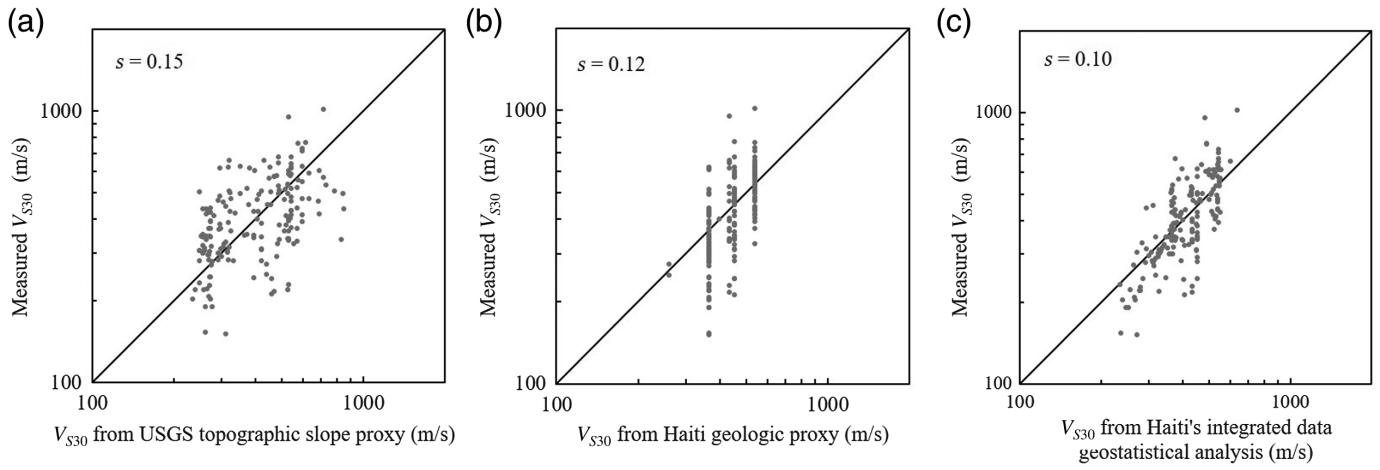

Figure 7. Plots of measured V_{S30} values versus (a) U.S. Geological Survey (USGS) topographic slope proxy-based V_{S30}, (b) geology-based V_{S30}, and (c) kriged V_{S30}. The base-10 logarithmic sample standard deviation (s) for each case is reported in the upper left corner.

in which h is the separation distance between the two points, σ^2 is the partial sill, Γ is the gamma function, v is the shape parameter, K_v is the modified Bessel function of the second kind of order v, a is the range parameter, and τ is the nugget. Subsequently, simple kriging is performed interpolating the trend's normalized residuals, and the resulting r_i is used to obtain the interpolated V_{S30} (V_{s30}^{kriged}) at each unsampled location in the gridded area as follows:

$$V_{s30}^{\text{kriged}} = \exp\left(r_i \times \sigma_{\ln(Vs30)}^{\text{geol}}\right) \times \left(V_{s30}^{\text{geol}}\right). \quad (4)$$

In Figure 7, the available in situ V_{S30} measurements in Haiti are plotted versus the V_{S30} values at the same locations from the USGS topographic slope proxy-based V_{S30}, Haiti's geologic proxy V_{S30} using the values presented in Table 1 and Haiti's kriged V_{S30} based on the integrated data (equation 4). The base-10 logarithmic sample standard deviation (s) for each case is presented in the upper left corner of each plot (Fig. 7), following Thompson *et al.* (2014) and Li *et al.* (2022). Thompson *et al.* (2014) obtained s values of 0.06 for their regression–kriging map at full resolution, and an s value of 0.11 corresponding to the geology-based map originally provided by Wills and Clahan (2006). Li *et al.* (2022) reported 0.21 and 0.15 for their kriged- and geology-informed V_{S30} values, respectively. Our kriged values also result in a reduction of variability, as seen in the previous studies. In relation to the aforementioned previous studies, our s values corresponding to kriged V_{S30} are larger than those from Thompson *et al.* (2014) yet lower than those from Li *et al.* (2022). The comparison presented in Figure 7 demonstrates the benefits in pursuing more extensive and robust subsurface characterization in the region.

Figure 7a shows scatter that is consistent with that reported by Thompson *et al.* (2014; though their s values were smaller). Topographic-slope proxy-based V_{S30} values (Wald and Allen, 2007) are particularly valuable in regions with scarce subsurface characterization like Haiti. Geology-informed V_{S30} values in Figure 7b show more scatter than their counterparts in Figure 7a. This distribution is due to the lack of evenly distributed V_{S30} measurements at some of the identified geologic units and the possible presence of outliers that cannot be rigorously identified due to the limited data available. For instance, some geologic units were represented by as few as one V_{S30} measurement, as shown in Table 1. Furthermore, a few measurements of V_{S30} were discarded, because these points were erroneously plotted in water bodies. This limitation can be addressed in the future by using a more detailed geologic map and more in situ measurements within all geologic units in Haiti. Figure 7c presents how the V_{S30} values extracted from the kriged analysis are in better agreement with the measured V_{S30} values (as evidenced by the smallest s value). This result was expected as the in situ V_{S30} measurements were incorporated in the kriging analysis as well as the geology-based V_{S30} at the unsampled locations grid, which means that s values could be artificially low in this case, because the model was trained and tested on the same dataset. Unfortunately, at the time of completion of this work, the scarce amount of V_S data in the region did not allow for separate training and validation sets. In the future, topographic slope proxy-based V_{S30} will be further integrated into the geospatial approach to investigate potential additional improvements in the reduction of the variability in estimated V_{S30} in the study regions.

Figure 8 presents the Port-au-Prince and Les Cayes' spatial distributions of the kriged V_{S30} values (Fig. 8a,b), the USGS topographic slope proxy-based V_{S30} (Fig. 8c,d), the ratio between the resulting kriged and topographic slope proxy-based V_{S30} surfaces (Fig. 8e,f), and the standard deviation associated to the kriged V_{S30} values (Fig. 8g,h). The kriged spatial distribution integrating the measured V_{S30} values and the geology-based V_{S30} for both the regions is presented within the maps overlaid

by the locations with measured V_{S30} in Figure 8a, b. The estimated and measured V_{S30} values are grouped based on the National Earthquake Hazards Reduction Program (NEHRP) site classification. The legend corresponding to locations classified as site class B (i.e., V_{S30} between 760 and 1500 m/s) show the actual maximum V_{S30} value (e.g., kriged V_{S30} only reach the maximum value of 910.3 m/s).

Integrating the available in situ V_{S30} measurements and the geology-based V_{S30} using kriging has shown an improvement in subsurface characterization, as seen in Figure 7c and Figure 8a,b. The capital city of Port-au-Prince provided another evaluation of the effectiveness of the integration of V_{S30} values from the geology, in situ measurements, and geospatial approaches. Figure 8a,c shows higher values of V_{S30} from the USGS slope-based V_{S30} compared to the kriged V_{S30} spatial distribution in the southern part of Port-au-Prince. It must be noted that there is a lack of measured V_{S30} data in that specific region, which highlights the importance of more subsurface characterization in that area. On the other hand, the kriged V_{S30} map of Les Cayes captures in more detail how the area is mostly within a NEHRP site class D (180–360 m/s), especially near the coast (Fig. 8b,d). This is consistent with the significant damage observed after the 2021 Nippes earthquake, particularly in Les Cayes, where sand boils were found in multiple locations close to structures that suffered considerable damage and even collapsed (Dashti *et al.*, 2022).

The ratio between the kriged V_{S30} and USGS topographic slope proxy-based V_{S30} distributions is shown in Figure 8e,f to illustrate the differences more clearly. Higher ratios (presented in dark red) represent areas where the kriged V_{S30} is higher than the USGS topographic slope proxy-based V_{S30}, whereas lower ratios shown in lighter shades represent lower kriged V_{S30} values. The differences could correspond to inherent limitations in proxy-based approaches, the limited V_{S30} measured values in the region, and potential bias in the data. For example, the differences in resolution of the kriged and USGS topographic slope proxy-based V_{S30} values can contribute to the observed differences. The USGS topographic slope proxy map has a 30 arcsec (~900 m spacing) resolution. Although our kriged V_{S30} map was created using a 500 m spacing grid to capture the variability of the locations with measured values as much as possible. The previous studies in locations with more robust data available (e.g., California and Texas) have used resolution grids of 3 arcsec (~90 m; Thompson *et al.*, 2014) and even 1 km (Li *et al.*, 2022). In addition, the V_{S30} geologic proxy values were obtained based on a 1:500,000 scale-geologic map (Wilson *et al.*, 2019). The use of a higher resolution geologic map can certainly improve the estimation of the geology-based estimates.

Although the spatial distribution shown in Figure 8g,h depicts the standard deviation (σ) associated with the kridged V_{S30} based on the standard deviations per geologic unit and the uncertainty from the kriging analysis. As expected, adjacent to the locations with measured V_{S30} values (shown by the black hollow circles), the uncertainties from the interpolation method decrease. For the remaining places distant from the locations with measured V_{S30} values, the distribution of σ tends to the distribution of the geologic conditions shown in Figure 6.

Site effects

A complete ground-motion characterization must include source, path, and site contributions to the amplitude, frequency content, and duration of the records of interest. In this study, we focus on investigating the role of local site conditions on the characteristics of recorded ground motions. Based on our characterization of the near-surface geologic conditions in Port-au-Prince (Fig. 8b), the geology-informed, kriged V_{S30} value at AY.NQUSE is 476 m/s. Insufficient data near AM.R50D4 did not allow for the computation of kriged V_{S30} values, but the topographic slope-based proxy at that location is 475 m/s (Dashti *et al.*, 2022). Because of the lack of reference rock motions and limited subsurface information at recording stations, comparative analyses between the mainshock and available ground motions from aftershocks recorded at the same station as well as single-station methodologies are implemented herein. The latter include the analysis of horizontal-to-vertical spectral ratios (HVSRs; Nakamura, 1989) based on earthquake ground motions at the stations that recorded the mainshock and the largest-magnitude aftershocks. The absence of measured V_S profiles at sites of interest limits the investigation of site effects via numerical site response analysis. However, the applications of HVSR provides a cost-effective approach to extract site-specific information, such as the site predominant frequency (Cox *et al.*, 2020; Zhu *et al.*, 2020; Wang *et al.*, 2022). After implementing signal processing protocols (i.e., gmprocess) on available records from 14 August 2021 until 28 August 2021, there were only two aftershocks for which the corresponding records had signal-to-noise ratio (SNR) larger than 3.0 over the frequency range between 0.1 and 10 Hz at AY.NQUSE. No ground motions from aftershocks recorded at AM.R50D4 had SNR larger than 3.0 between 0.1 and 10 HZ. Hence, we only evaluate potential site effects at station AY.NQUSE by comparing HVSRs (i.e., computed with the entire time series per record) from the mainshock and the two aftershocks listed in Table 2.

Table 2 provides the focal depths, magnitude, and magnitude types for each one of these events. In addition, Table 2 presents the corresponding location of the epicenter of each event, epicentral distance, as well as the PGA_{ROTD50} and PGV_{ROTD50}. The aftershock that occurred on 15 August 2021 with a magnitude of 5.8 was the largest aftershock of the 2021 Nippes earthquake (Calais *et al.*, 2022).

Values of HVSRs are computed based on the Fourier amplitude spectrum (FAS) of observed ground motions, which were

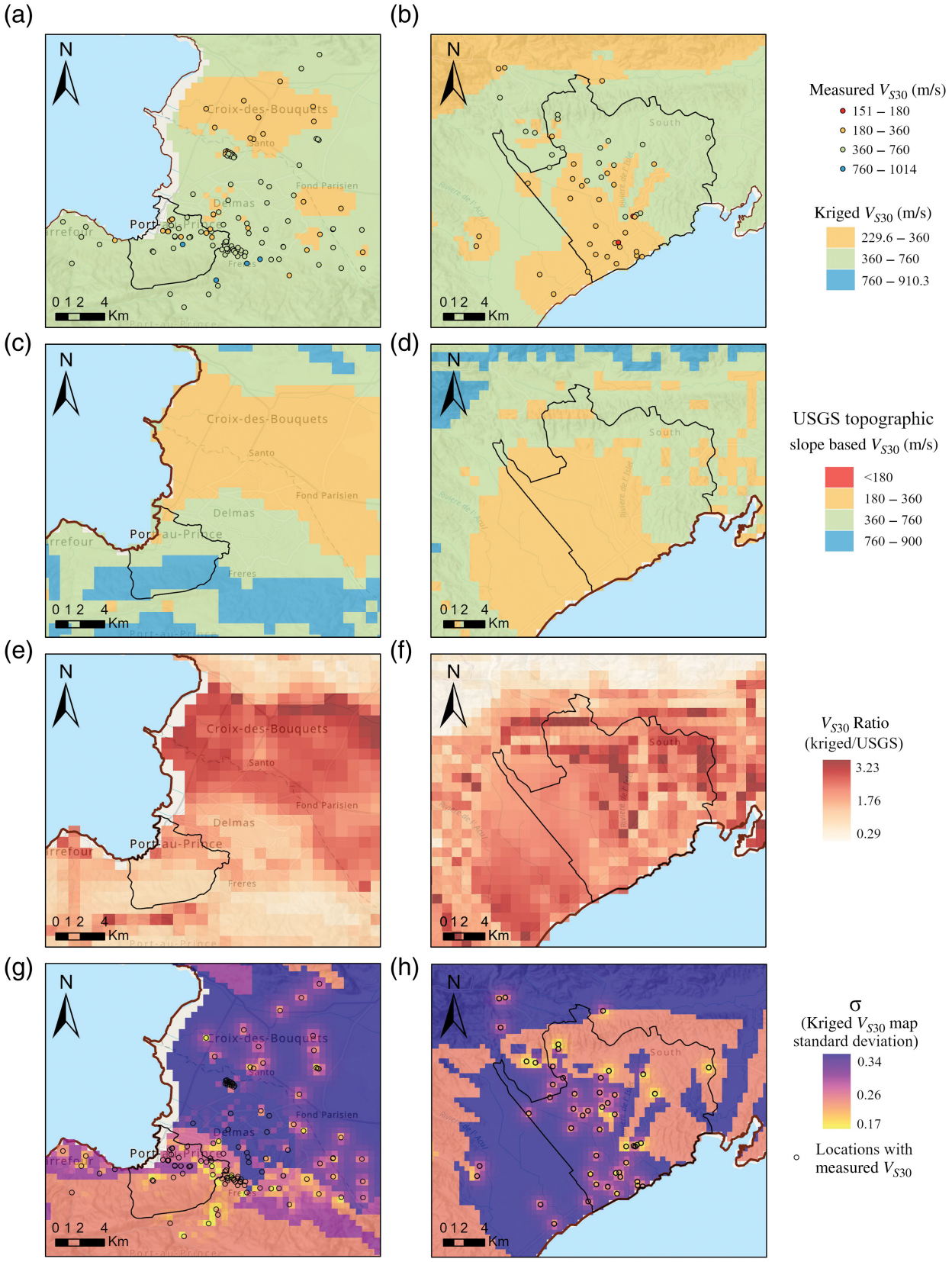

Figure 8. Port-au-Prince (left) and Les Cayes (right) with mapped spatial distributions of (a,b) kriged V_{S30}, (c,d) USGS topographic slope proxy-based V_{S30}, (e,f) ratio between the kriged and USGS topographic slope-based V_{S30} maps, and (g,h) standard deviation associated to the kridged V_{S30} map. The color version of this figure is available only in the electronic edition.

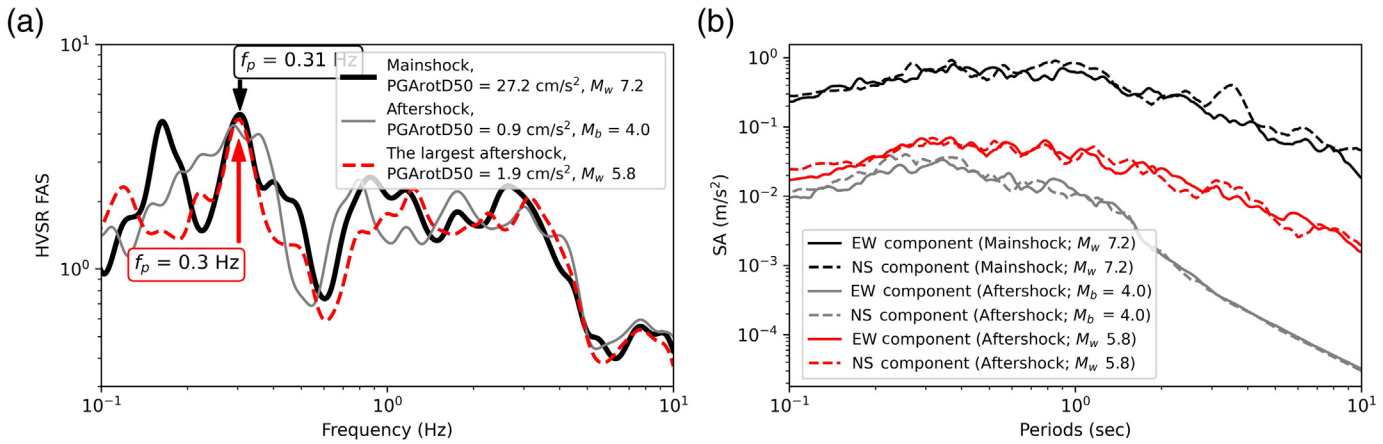

Figure 9. (a) Horizontal-to-vertical spectral ratio (HVSR) and (b) 5%-damped response spectra of the EW and NS components of the mainshock and two aftershocks recorded at the AY.NQUSE. The color version of this figure is available only in the electronic edition.

smoothed by a Konno–Omachi filter with a value of 30 for the b coefficient (Konno and Ohmachi, 1998) as follows:

$$\mathrm{HVSR}=\frac{\mathrm{FAS}_{\mathrm{H,geo}}}{\mathrm{FAS}_{\mathrm{V}}}, \tag{5}$$

in which $\mathrm{FAS}_{\mathrm{H,geo}}$ is the geometric mean of the two recorded horizontal components smoothed FAS, and $\mathrm{FAS}_{\mathrm{V}}$ is the smoothed FAS for the vertical component. Figure 9a shows the HVSR for the three ground motions recorded at AY.NQUSE. The black, solid line depicts the HVSR values corresponding to the mainshock with $\mathrm{PGA}_{\mathrm{ROTD50}}$ of 27.2 cm/s^2, and the red dashed line represents the largest aftershock with $\mathrm{PGA}_{\mathrm{ROTD50}}$ of 1.9 cm/s^2. The gray line corresponds to the aftershock with $\mathrm{PGA}_{\mathrm{ROTD50}}$ of 0.9 cm/s^2. Figure 9a shows clear peaks from the mainshock and the two aftershocks at around 0.3 Hz, which could be explained by site effects. An additional peak is observed at 0.16 Hz in the HVSRs corresponding to the mainshock that is not present in the aftershocks. This observation may suggest that the peak at 0.16 Hz results from a source characteristic rather than a site effect. Peaks at higher frequencies are generally less reliable, but the coincidence of peaks among the mainshock and aftershock at higher frequencies (as shown in Fig. 9a) is also indicative of potential site effects due to near-surface sediments.

To further investigate the site response at AY.NQUSE, the 5%-damped response spectra for the mainshock and two aftershocks are calculated and compared in Figure 9b in log–log scale. The EW and NS components' spectral accelerations corresponding to the aftershocks are similar, which may suggest a source contribution to the polarization observed in the ground motions from the mainshock. The amplitudes of the response spectra reflect very different ground shaking intensities as a result of low-to-moderate magnitude aftershocks considered in this study. Hence, the response spectra for the NS and EW components are normalized by their corresponding maximum amplitude and shown in Figure 10.

In Figure 10, we observe that spectral shapes corresponding to all the three ground motions are similar. Particularly, predominant periods for the EW and NS components of the mainshock and aftershocks are around 0.3 s (for both components), which may be related to a systematic contribution of the site conditions. The spectral shape of the NS component has a second peak (of comparable amplitude with respect to the maximum peak at around 0.4 s) around 1s that does not appear in the EW components of neither the mainshock nor the aftershocks. Moreover, a bump is observed at about 4 s for the NS component of the mainshock only.

TABLE 2
Characteristics of the Ground Motions Recorded From the 2021 Mainshock and Corresponding Aftershocks at AY.NQUSE

Earthquake Time (UTC) (yyyy/mm/dd hh:mm)	Latitude (°)	Longitude (°)	Focal Depth (km)	Magnitude	Magnitude Type	Backazimuth (°)	Epicentral Distance (km)	$\mathrm{PGA}_{\mathrm{ROTD50}}$ (g%)	$\mathrm{PGV}_{\mathrm{ROTD50}}$ (cm/s)
2021/08/14 12:29	18.43	−73.48	10.00	7.2	*M_{ww}	260.92	131.11	2.78	4.82
2021/08/14 12:45	18.56	−73.75	13.43	4.0	†M_b	270.00	158.63	0.09	0.06
2021/08/15 03:20	18.40	−74.09	8.32	5.8	*M_{ww}	264.89	195.38	0.19	0.30

*M_{ww} indicates generic seismic moment magnitude.
†M_b indicates body wave magnitude.

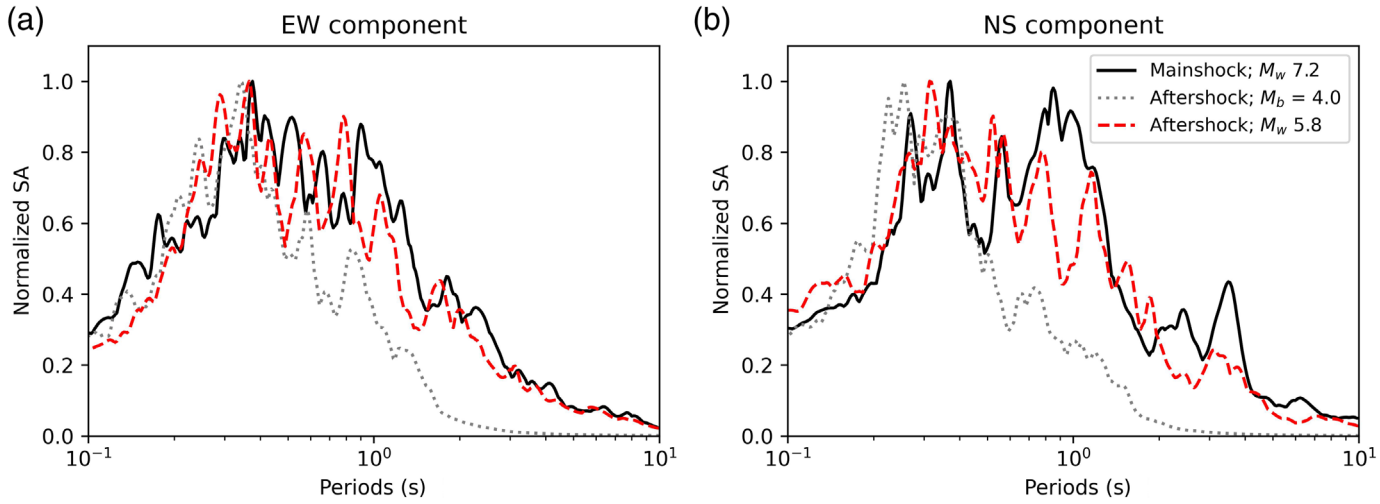

Figure 10. Normalized (5% damped) response spectra of the (a) EW and (b) NS components of the mainshock and two aftershocks recorded at the AY.NQUSE. The color version of this figure is available only in the electronic edition.

GROUND FAILURE OBSERVATIONS

Secondary earthquake hazards such as earthquake-induced landslides, rockfalls, and debris falls can have a significant effect on critical infrastructure. These hazards inhibit immediate recovery following an event and, in the long term, can have socioeconomic impacts, including obstructing access to markets, healthcare, and education (Whitworth *et al.*, 2020a; Jones *et al.*, 2020). The potential impacts of these hazards are exacerbated by east–west migration following the 2010 earthquake (Whitworth *et al.*, 2022). In addition to earthquake-induced landslides, liquefaction and lateral spreading impacted transport infrastructure and urban developments. A GEER team undertook a site reconnaissance on 9–10 October 2021, to evaluate evidence of ground failures and their geotechnical impacts along critical infrastructure routes RN7 between Les Cayes and Jérémie and along Communal Route 204-A (RC-204A) and National Route 2 (RN2) around L'Asile, Balou, and Cavaillon. Ground failure observations after the 2021 Nippes earthquake fell into three general categories: landslides (including isolated slope failures and large-scale translational earth slides), rockfalls, and lateral spreading due to soil liquefaction or cyclic softening in the underlying soil. In some cases, further site investigation is necessary to identify the exact mechanism of ground failure. However, possible causes are hypothesized based on the existing evidence. Evidence of earthquake surface fault rupture was ultimately deemed inconclusive. The collected data are used herein to characterize the ground failures. It can be further utilized to evaluate the resilience of infrastructure to this and future earthquakes by assessing the efficacy of landslide mitigation measures, and understanding the vulnerability of major settlements to liquefaction (UN International Strategy for Disaster Reduction [UNISDR], 2013; Whitworth *et al.*, 2020b). These assessments can improve infrastructure resilience and postevent recovery.

Earthquake-induced landslides, rockfalls, and debris falls

The 2021 mainshock triggered several large landslides and localized slope failures throughout Haiti's southwestern peninsula. Satellite imagery shows significant landslide activity in the mountainous terrain of Pic Macaya National Park, primarily caused by the mainshock with smaller impact from the 16 August arrival of Tropical Storm Grace. Because of safety and accessibility concerns, on-site reconnaissance of Pic Macaya National Park was not possible. The on-site GEER team did identify over 30 instances of fanning debris cones along RN7 containing mostly colluvium (Fig. 11a), boulders amongst colluvium (Fig. 11b), and rockfalls with boulders estimated to be as wide as 5 m (Fig. 11c). The large extent of landslide and rockfall damage along RN7 poses a significant hindrance to postevent recovery, because RN7 is the only direct lifeline connecting the heavily populated region around Les Cayes through Pic Macaya National Park northward to the Grand'Anse department. Despite the extensive road network of Haiti's southwestern peninsula, a single road (i.e., RN7) crosses the boundary between the south and Grand'Anse departments. Evidence remained of complete road blockages along RN7 upon the arrival of the GEER team in Les Cayes, with two examples shown by the debris in Figure 11a,b, and the large boulder and debris still blocking both the lanes of RN7 in Figure 11c. Given logistical constraints of rapid reconnaissance during the COVID-19 pandemic, the GEER team was unable to note the amount of time required to clear debris and make RN7 passable again. Instead, much of the debris was already cleared upon arrival, yet slide debris in many locations still crossed at least one lane of RN7 (e.g., Fig. 11a).

The GEER team observed several examples of rockfall damage to gabion retaining walls on the sides of RN7. For instance, the concrete linings atop a gabion wall appeared to have been crushed under the impact of boulder debris (Fig. 11d,e), which

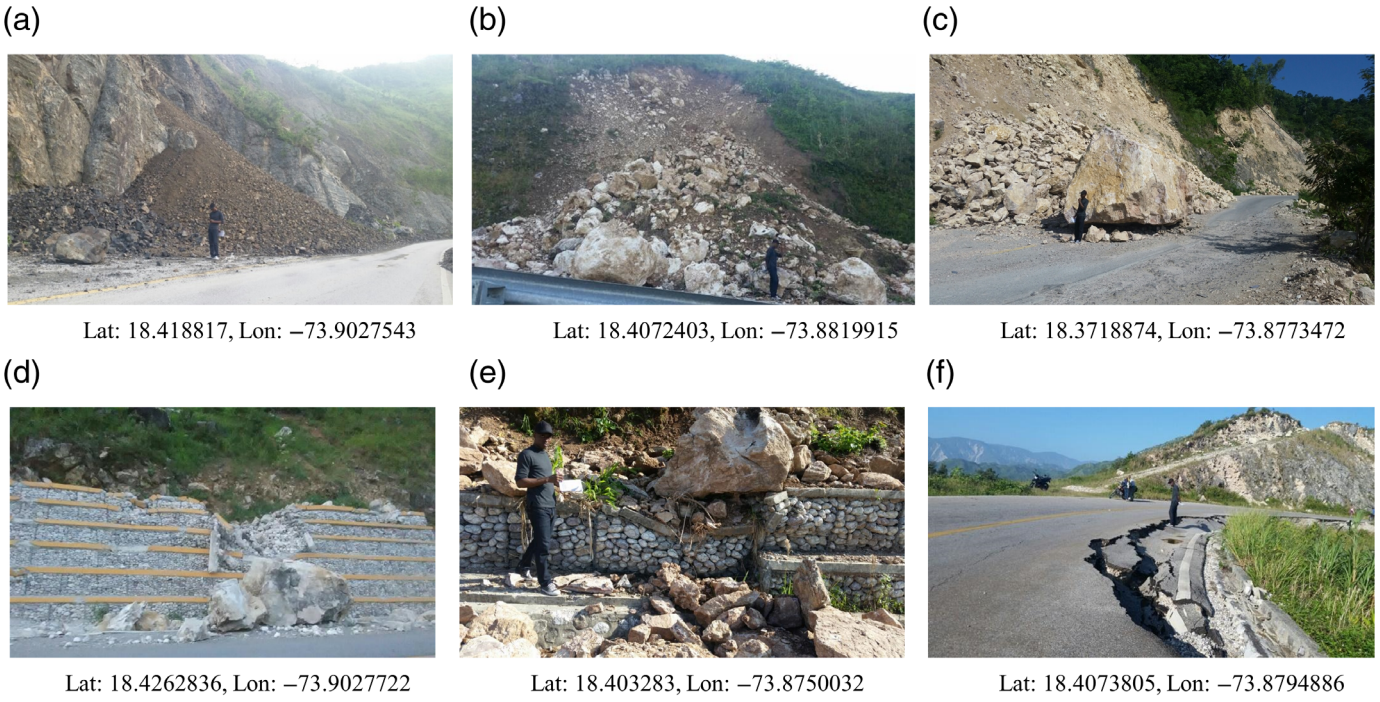

Figure 11. Examples of slope failure impacts along RN7: (a–c) small, mixed, and large grain sizes; (d,e) gabion wall damage observations; (f) slope displacement damage to highway pavement. Photographs in panels (a,b,c, e,f) courtesy of Joseph Emmanuel Dessable. Photograph in panel (d) courtesy of Marvens Logiste. The color version of this figure is available only in the electronic edition.

in turn pushed the rocks within the gabion cages outward. Although the gabion walls exhibited crushing at their surfaces due to debris impacts, the GEER team did not identify any toppling or translation of the walls due to slope failures or backfill pressure. Despite the damage to the gabion walls themselves, their presence may have had a mitigating effect on the road blockages caused by rockfall and landslides by slowing down falling debris and preventing it from crossing both the lanes of RN7. Figure 12 shows the results of 2D slope rockfall analyses performed using the software RocFall2 (Rocscience, 2021). Analyses were performed with and without a gabion wall, as shown in Figure 13a,b, and with rocks having diameters of 0.5and 1.5 m and symmetric shapes consistent with the boulder shapes observed in the reconnaissance. Figure 12b shows that the presence of a gabion wall significantly hindered the trajectory of rock debris, causing significantly more rocks to come to rest at locations behind the wall or immediately adjacent to the wall as compared to when no gabion wall is present. The effect of the gabion wall on the trajectory of the rock debris is less significant for larger rocks having diameters of 1.5 m. The results of the RocFall2 analyses provide a possible explanation for why examples of entire lane blockages, as seen in Figure 11a–c, were not observed adjacent to gabion retaining walls.

The on-site GEER team also documented evidence of seismic slope displacement in the form of slope-parallel pavement cracks at seven different locations, one of which is shown in Figure 11f. Additional slope-parallel cracks were observed 2–3 m downslope from the image in Figure 11f. The exact cause of the cracks, that is, whether due to cyclic softening, lateral spreading, or limited seismically induced slope displacement, is not known at this time.

The GEER team documented two ground failures in close proximity to the EPGF along a 16 km stretch of RC-204A. The images in Figure 14a,b near L'Asile show open fissures and a headscarp approximately 2 m in height. These are likely a result of cyclic mobility or cyclic softening. Further west toward Balou, a rockfall and ground rupture were observed. This rupture shown in Figure 13c is possibly caused by earthquake surface fault rupture, given its proximity to the EPGF (approximately 70 m), but evidence of earthquake surface fault rupture was ultimately inconclusive.

Liquefaction triggering and effects

Cyclic softening and lateral spreading. The GEER team found several ground fractures and open fissures during their reconnaissance (Dashti *et al.*, 2022). Some of them occurred within 50 m of a river and showed evidence of sand ejecta (Fig. 14a), which suggests that they resulted from lateral spreading. Other fractures, such as the one shown in Figure 14b, occurred in quaternary alluvium adjacent to a river. This ground failure (Fig. 14b) also occurred within 100 m of the main trace of the EPGF and showed no evidence of sand ejecta. Further investigation is necessary to determine, if this feature may instead be evidence of earthquake surface fault rupture. Additional liquefaction-related damage was observed

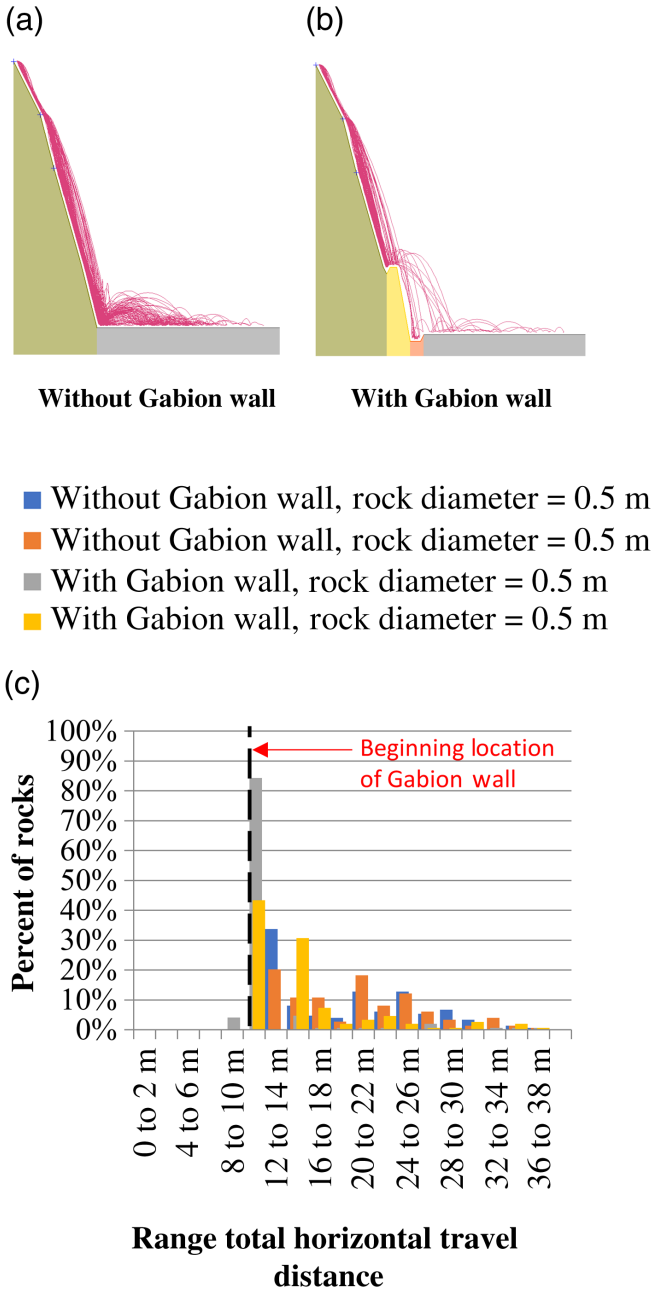

Figure 12. (a,b) Slope geometry used in rockfall analyses with and without the presence of a gabion wall. Red lines indicate travel paths from each iteration of the rockfall analyses. (c) Histograms of resting locations from all rockfall analyses. The color version of this figure is available only in the electronic edition.

in urbanized regions of Les Cayes and Pestel. Figure 14c shows cracks along a wharf in Pestel that appear similar to cracks induced by lateral spreading observed in port facilities in Port-au-Prince after the 2010 Haiti earthquake. However, the subsurface at this location is primarily Eocene rock rather than the quaternary alluvium at other locations of liquefaction observations.

Likelihood of liquefaction. An evaluation of the likelihood of liquefaction manifestation in Les Cayes was performed using a simplified SPT-based liquefaction triggering procedure (Boulanger and Idriss, 2014), based on five available SPT boreholes (BLC1-BLC5) provided by the State University of Haiti (see Data and Resources). All boreholes were located near coast of Les Cayes, where the groundwater table is located about 1 m below the surface. In the absence of a nearby reliable ground motion station, a peak ground acceleration (PGA) of 0.35*g* was estimated from the USGS PGA Shakemap (see Data and Resources). The liquefaction potential index (LPI; Iwasaki, 1978) was also estimated for each soil profile. Figure 15 shows the field SPT-N measurement and liquefaction triggering analysis results for each borehole. In general, the presence of quaternary alluvial deposits at the city of Les Cayes makes the region particularly susceptible to liquefaction triggering and related geohazards, such as lateral spreading.

The simplified soil profiles for boreholes BLC1, BLC2, and BLC3 showed that the first 1–2 m thick hydraulic fill layer and the thicker silty sand layer are susceptible to liquefaction. The LPI values ranged from 24 to 32.5, indicating that major damage (i.e., LPI > 15) was expected. This is consistent with the field observations of possible lateral spreading near south Les Cayes. The main liquefiable layer for boreholes BLC4 and BLC5 was identified at 12–14.5 m. The LPI values for these two boreholes were around 2, indicating that minor damage (i.e., LPI < 5) was expected in this area. Additional field and laboratory testing data are required to better identify the impact and extension of liquefaction hazard.

SOCIAL SCIENCE OBSERVATIONS

Vulnerability to multiple natural hazards

As noted earlier, natural hazards pose a threat to about 96% of Haitians (World Bank, 2021). The country is vulnerable to earthquakes and heavy storms during hurricane season (1 June–30 November 30). Between 2020 and 2021, disasters killed 233,562 Haitians (see Data and Resources), 96% and 3% of which were linked to earthquakes and hurricanes, respectively. The remaining losses were caused by floods, droughts, and epidemics, among others. Following the 2010 M_w 7.0 earthquake, which claimed 222,570 lives (see Data and Resources) and displaced over 1.5 million people (World Bank, 2019), the 2021 Nippes earthquake was Haiti's most recent major disaster killing more than 2200, injuring over 12,500, and leaving close to 650,000 in need of humanitarian assistance (see Data and Resources). As shown in Figure 1, other catastrophic events have severely impacted the country. From 2014 to 2016, natural hazards, such as Hurricane Thomas, Isaac, Sandy, and Matthew, affected close to 58% of the population in each of the country's ten departments. Lack of adequate administrative capabilities and a fragile economic state make Haitians more vulnerable to disasters (World Population Review, 2021).

Figure 13. (a) Landslide debris looking downslope and (b) headscarp shown with a 1.6 m tall person for scale. (c) Possible surface fault rupture next to RC-204. Photographs courtesy of Tarah Jeannot. The color version of this figure is available only in the electronic edition.

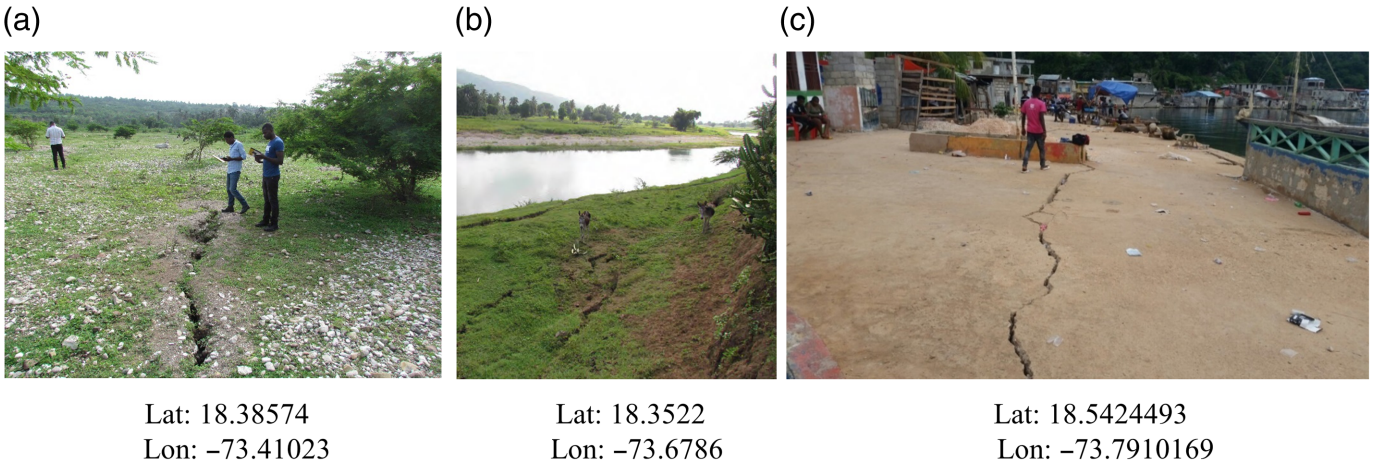

Figure 14. (a) Surface cracks with evidence of sand ejecta immediately adjacent to the cracks (courtesy of Newdeskarl Saint Fleur). (b) Lateral spreading observed near the free face along Rivière de Cavaillon (courtesy of Newdeskarl Saint Fleur). (c) Cracking along the wharf in Pestel (courtesy of Joseph Emmanuel Dessable). The color version of this figure is available only in the electronic edition.

Beyond natural hazards, other risks, including the COVID-19 pandemic have significantly impacted communities in Haiti. By 14 August 2021, Haiti had recorded a total of 20,719 of COVID-19 cases and 583 deaths. According to 15 February 2022 report from the Haitian Ministry of Health (Ministère de la Santé Publique et de la Population), the total number of COVID-19 cases rose to 30,208 and deaths to 819 (see Data and Resources). The relatively low numbers compared to that of other countries have puzzled many, given the low recorded vaccination rate. The impacts of this exposure are further exacerbated when considering vaccination inequities across the island and the globe. Until 15 July 2021, Haiti was the only country in the America without a single dose of the COVID-19 vaccine. Between 15 July and 21 September 2021, approximately 61,204 of the 500,000 COVID-19 vaccination doses supplied by the U.S. were administered, vaccinating 18,987 Haitians (see Data and Resources). As of February first, 2022, an estimated 100,126 individuals have been fully vaccinated (see Data and Resources). This number, however, does not account for individuals who traveled abroad to get their shots.

Governance challenges

Haiti, the first "black republic" and the second independent nation in the America's Fanning (2007), is now identified as a fragile state, where it is unable to provide fundamental amenities to their citizens, such as education, health care, clean water, and security (Collier, 2008; World Bank, 2011; Pritchett *et al.*, 2013). Among the reasons behind this fragility of the Haitian state is the government's strong reliance on nongovernmental organizations (NGOs)

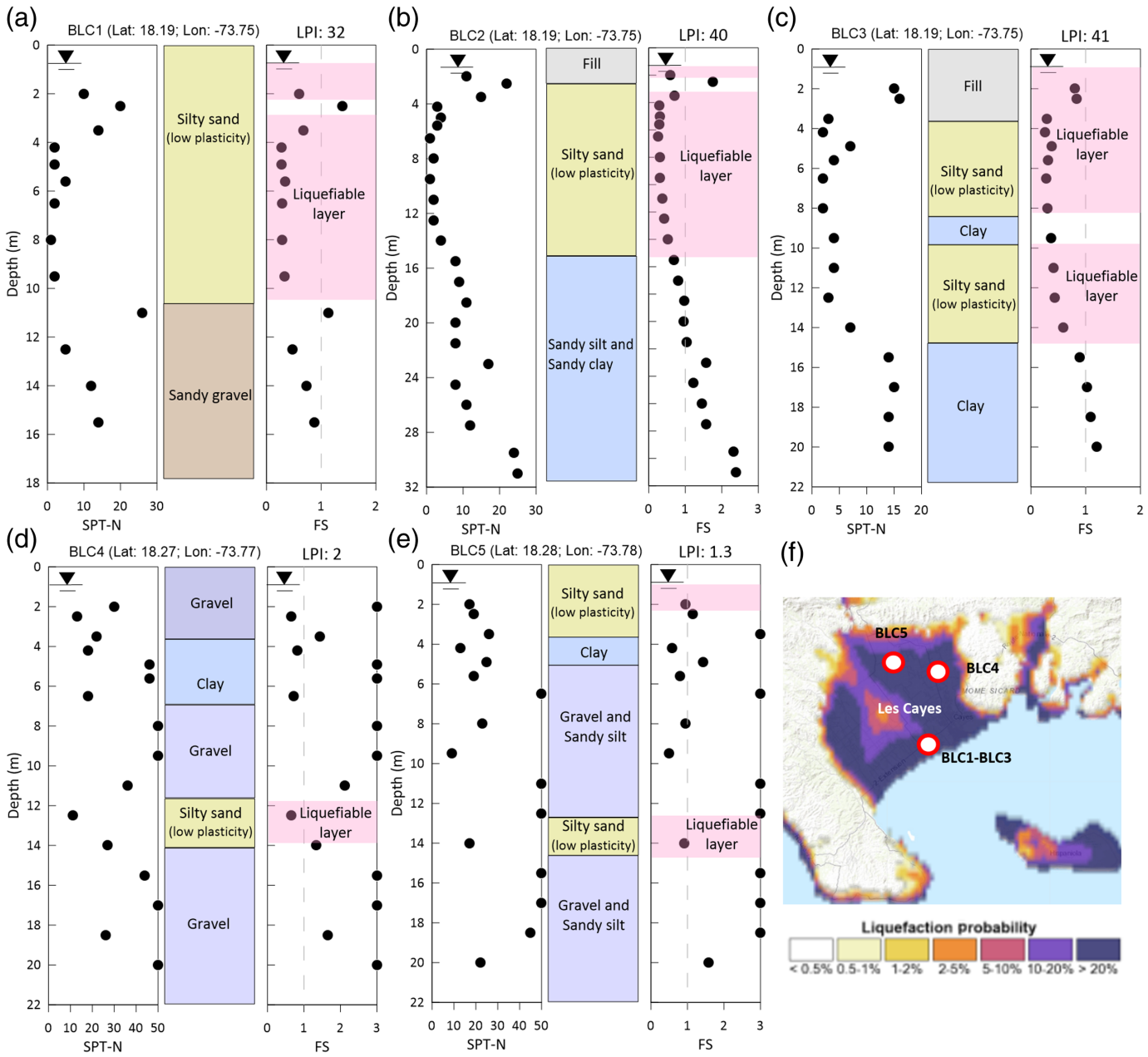

Figure 15. Field SPT-N measurements and liquefaction triggering analysis results for: (a–c) boreholes BLC1-BLC3 (near the south coast of Les Cayes); (d–e) boreholes BLC4-BLC5 (near the north of Les Cayes); and (f) the USGS liquefaction probability map at Les Cayes. The color version of this figure is available only in the electronic edition.

and international aid (Zanotti, 2010; Marcelin *et al.*, 2016; Dashti *et al.*, 2022), the lack of political legitimacy and administrative capability (Brière *et al.*, 2010), the prevalence of endemic corruption (Fatton, 2002), the absence of rule of law, and the dominance of impunity (Marcelin and Cela, 2020). The cycle of political crisis and economic instability extends the governance challenge in the country. Since category 4 Hurricane Hazel in 1954, close to 90 NGOs operated in Haiti (Schuller, 2017). This was considered the first wave of NGOs in the country. By 2009, an estimated 8000–9000 NGOs were recorded in Haiti (Hallward, 2007), which earned the country the nickname of the "Republic of NGOs" (Kristoff and Panarelli, 2010; Bradley, 2012). Following the 2010 earthquake, many discussions emerged on NGO contributions and accountability. This included high operational costs (Kwok, 2016), failure to deliver on reconstruction promises (Sontag, 2012; Elliott and Sullivan, 2015), and activities that undermined the Haitian Government.

Although the impacts of the 2021 earthquake were less severe than the 2010 earthquake, the most recent event has compounded the difficulty of addressing ongoing repair needs from the previous disasters, while also managing the current safety and security challenges facing those working in the country during a global pandemic.

Security challenges

Haiti has seen several UN peacekeeping missions to bolster the rule of law in institutions such as the Haitian National Police and law institutions since 2004. Despite these efforts, security in Haiti has continued to crumble. These issues were further exacerbated in 2020, with an uptick in kidnappings, gang violence, civil unrest, and protests against the government, coupled with unemployment, food insecurity, fuel shortages, and the COVID-19 pandemic (Human Rights Watch, 2020; Mérancourt and Faiola, 2021). According to a 2022 report by Insight Crime, the year of 2021 was the most violent one since the 1986 coup (see Data and Resources). With powerful and violent criminal gangs occupying about 60% of the capital and surrounding areas, access to roads and ports have been disrupted. Of the 1630 homicides recorded in 2021, an estimated 74% occurred between January and September (see Data and Resources). Since the assassination in 2021 of former President Jovenel Moïse, the level of gang violence has reached unprecedented levels. According to a May 2022 report from cable news network, this new reality has blocked main arteries that connect major cities, led about a dozen of medical centers and over 400 schools to close (see Data and Resources). Unstable political conditions are further exacerbated by high inflation and food insecurity.

Developmental challenges

Haiti's postearthquake challenges are unprecedented not only because of its governance and security challenges but also because of its ongoing developmental challenges. The country has experienced minimal annual Gross Domestic Product (GDP) growth in 1990 and 2000, followed by negative annual GDP growth both in 2010 (−3.8%) and 2020 (−3.4%). The roots of Haiti's developmental challenges date back to the 1800s after proclaiming its independence in 1804 and being one of the wealthiest French colonies making more money for France than all the other 13 French colonies (McKey, 2016). However, Haiti was obligated to pay reparations to France to maintain its independent status and gain immunity from the French military invasion. Haiti took 122 yr to pay this debt, estimated at $21 billion, and finally settled in 1947. Subsequent multiple shocks have battered the country since, including foreign intervention, political instability, and disasters.

Haiti relies heavily on foreign aid and external remittance. Foreign aid accounts for over 20% of the Haitian government's annual budget, which was $3.7 billion for 2020–2021 (Le Nouvelliste, 2021). Remittance sent to Haiti represents about 25% of the GDP (see Data and Resources), up from 8.42% of the country's GDP in 2000 (see Data and Resources).

In 2020, Haiti ranked 170 out of 189 countries in the United Nations Development Program (UNDP) Human Development Index, down from 163 in 2015 (UNDP, 2015) and 149 in 2009 (UNDP, 2009). According to the World Bank (2021), Haiti is one of the most unequal countries in the Americas. The poverty rate is nearly at 60%, with two-thirds of the poor living in rural areas (World Bank, 2021). About 38% lack access to acceptable water and 76% live with inadequate access to sanitation (UNDP, 2020). An estimated 25% of the population is illiterate (UNDP, 2020). The lack of affordable and good education, ongoing political unrest, and the COVID-19 pandemic have prevented four million (70%) children from attending school during the 2019–2020 academic year alone.

Mental health challenges

The concurrent disasters in Haiti present complex and long-term impacts on the Haitian population. Many are forced to relocate to safer regions, social networks and schooling are disrupted, and life is no longer the same (Shultz *et al.*, 2016). Women are particularly impacted by those challenges. Studies conducted in Haiti indicated a higher prevalence of mental health symptoms among women compared to men (Blanc *et al.*, 2016; Joshi *et al.*, 2021) and increased incidences of sexual violence toward them (Willman and Marcelin, 2010; Fanm, 2012; Rahill *et al.*, 2015, 2020). Traumatic life-changing events, such as, breakdown of social infrastructure, separation from parents or parental death, and displacement of families associated with disasters, increased the vulnerability of an estimated 500,000 children (CDC and Interuniversity Institute for Research and Development [INURED], 2014).

INTERSECTION OF SOCIAL SCIENCE AND ENGINEERING

Social science observations are interlinked to geotechnical impacts investigated in Haiti after the 2021 Nippes earthquake in multiple ways. First, Haiti's concurrent crises (e.g., earthquakes, hurricanes, the COVID-19 pandemic, security challenges, etc.) are often followed by a response-oriented humanitarian involvement in Haiti, as opposed to one that has a long-term developmental focus that might reduce Haitians' vulnerability to natural hazards. Studies show that the majority of monetary aid in Haiti was allocated to humanitarian and security related efforts from 2002 to 2008, resulting in minimal investments being applied to long-term development and sustained strategic planning (Fischer and Levy, 2012). This issue was further exacerbated after the 2010 earthquake, as many of the organizations and much of the external assistance that came to Haiti were response oriented, focusing more on providing relief from the earthquake and cholera crises, and not on establishing longer term development programs (Gelting *et al.*, 2013; Ramachandran and Walz, 2015).

Second, given Haiti's current and multifaceted crises, preparing for uncertain natural hazards (for which corresponding return periods are often articulated in probabilistic terms not readily understood by most of the population, and for which impacts on the built environment and communities, i.e., risk, are also uncertain) can be unrealistic for many, as shown in other contexts (Pérodin *et al.*, 2021). Most families already

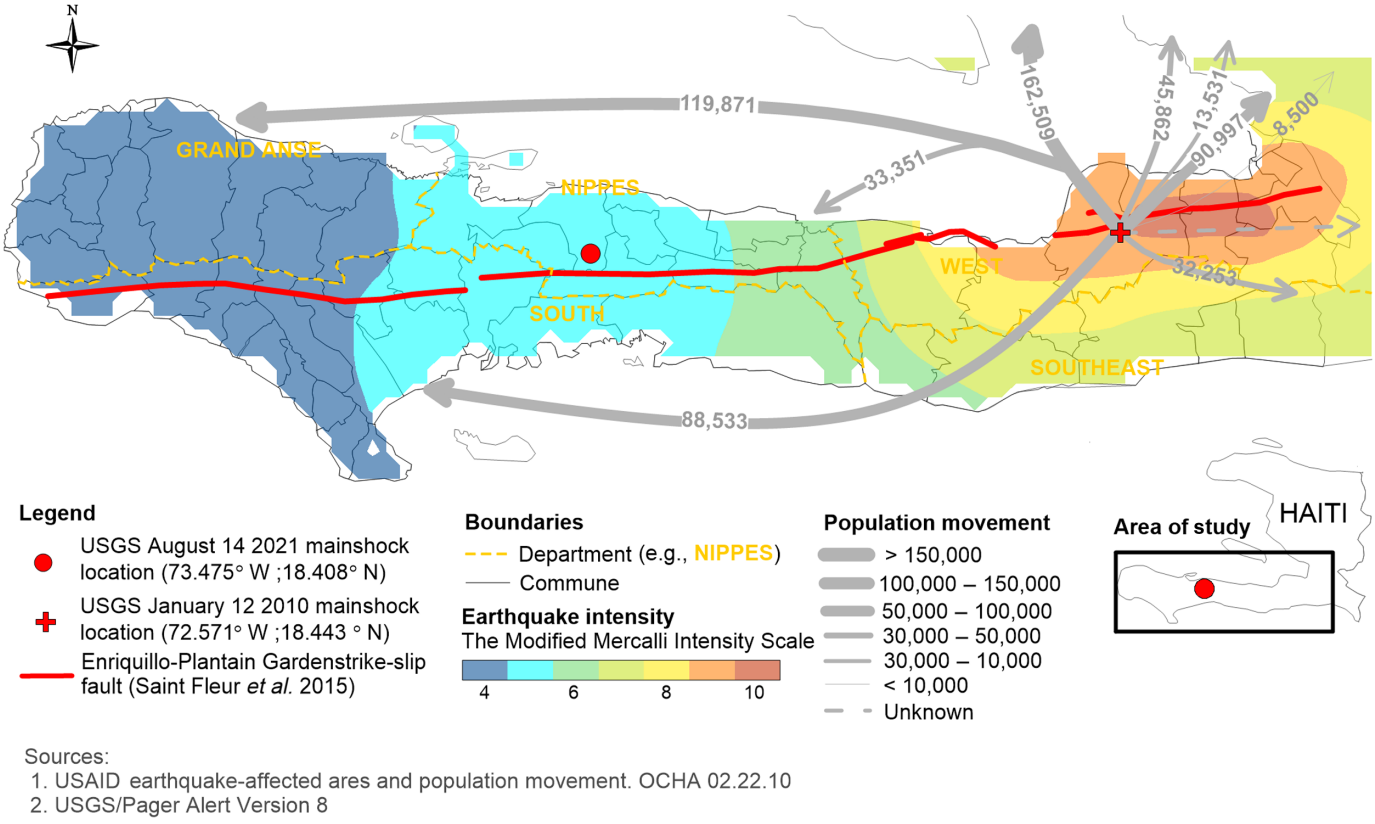

Figure 16. Intersectional map of population movements following the 2010 earthquake in Haiti (sources noted in the legend) and the spatial distribution of the earthquake intensity corresponding to this event. The color version of this figure is available only in the electronic edition.

struggle to meet their day-to-day needs amid extreme poverty, on top of their struggle to survive amid the new gang battle. Our earlier work (Ganapati and Rahill, 2017) also showed a complex role played by faith in disaster preparedness in Haiti. After the 2010 earthquake, for instance, some Haitians believed that the 2010 earthquake was the beginning of the end of the world, and that all they should do was to "eat", "drink", and "pray". In their minds, there was not much they could do in the face of these calamities. Effective science communication and educational programs are essential in these settings to increase earthquake preparedness and community resilience. Collaborative work between scientists, NGOs, and higher education institutions in Haiti could provide a vehicle for integrated approaches, in which the assessment of seismic hazards (and other natural hazards), their impact on the built environment from an engineering perspective, and on communities from a social sciences perspective are all considered in recovery and resilience plans.

Third, as a fragile state, prior to the 2010 earthquake, the country lacked a building code as well as the infrastructure necessary for identifying areas vulnerable to seismic hazards (e.g., in-country seismologists, seismic hazard maps, microzonation, or a robust seismic network) (Calais *et al.*, 2019). This meant that both Haitian government officials and the public had access to "limited information" on seismic risks. A socio-seismology experiment conducted in Haiti revealed, for instance, that 93% of the study's respondents desired to have more earthquake-related information, including information on seismically vulnerable areas and earthquake-resistant construction practices (Calais *et al.*, 2020).

Fourth, extreme poverty and the presence of NGOs play a significant role in driving migration patterns and the formation of internally displaced persons (IDP) camps, in most cases in areas vulnerable to natural hazards (see Figs. 16 and 17). The mere presence of NGOs dictates where IDP camps form, drawing the displaced to gain access to food, water, shelter, and medical care. After the 2010 earthquake, hundreds of thousands of Haitians erected shelters made of scrap material in highly visible, urban locations near to NGOs (Desvarieux and Harris, 2010). These ad hoc communities, called "tent cities", took shape on empty lots, hillsides, and pastures without consideration of the IDP camp's geographic appropriateness, seismic safety, or its vulnerability to other natural hazards (e.g., hurricanes and floods).

Intersectional maps

A few days after the January 2010 earthquake in Haiti, the death toll reported by the government exceeded 230,000. The U.S. Agency for International Development (USAID) reported more than 1,200,000 people displaced and about 3,000,000 affected (see Data and Resources). Nearly a month

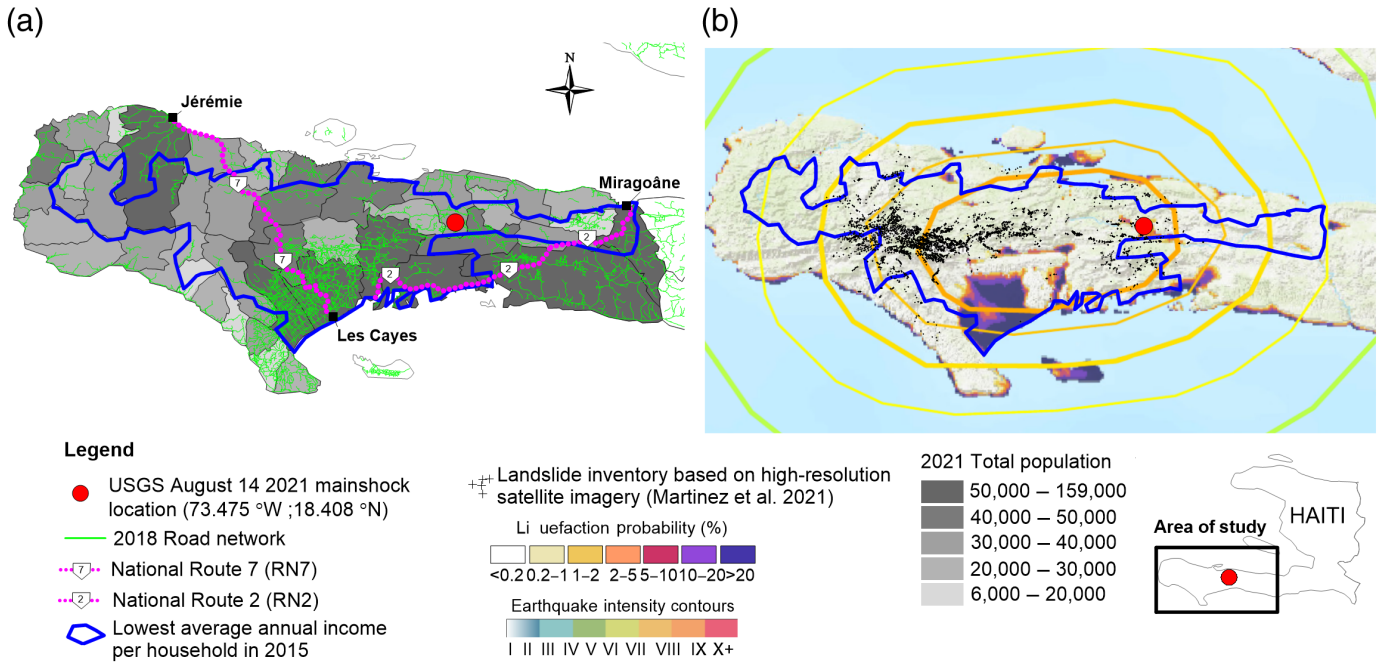

Source: Center National de l'Information GeoSpatiale (CNIGS), UNDAC, OpenStreetMap. Created by MAP Action on 22/09/2021. https://mapaction.org
USGS ground failure maps. Last updated 19 August 2021
https://earthquake.usgs.gov/earthquakes/eventpage/us6000f65h/ground-failure/summary
2018 Road network from Center National de L'Information Geo Spatiale (CNIGS)

Figure 17. Intersectional maps depicting: (a) 2021 population map with the boundary of the lowest average annual income within the study region in Haiti (sources noted in the legend). The road network map is also shown highlighting important lifelines such as National Route 7 (RN7), which was affected after the 2021 earthquake. (b) The USGS liquefaction probability map, earthquake intensity contours of the 2021 Nippes earthquake, and a landslide inventory map (Martinez *et al.*, 2021) overlaid on the boundary of the lowest average annual income. The color version of this figure is available only in the electronic edition.

after the disaster, the USAID estimated that over 500,000 had left Port-au Prince to other provinces within Haiti (see Data and Resources). The Grand'Anse and southern regions were the second- and third-most popular destinations for many Haitians. Figure 16 shows the intersection of social and engineering observations. This type of maps is, hereafter, referred to as intersectional map. Specifically, Figure 16 depicts population movement following the 2010 earthquake and the earthquake intensity contours corresponding to that event. The exodus after the 2010 earthquake exposed a greater population to the seismic hazards and associated geohazards of the 2021 earthquake in view of the proximity to the epicenter of the Nippes earthquake, locations of greater shaking intensities, landslides, and liquefaction-prone coastal regions. According to the Internal Displacement Monitoring Centre (2020), many of those displaced internally by the 2010 earthquake returned to their place of origin. Those who decided to stay in campsites in Port-au-Prince did so because the living conditions at their place of origin were not better. Historically, Haiti has dealt with challenges from centralization. Because local farming was no longer sustainable, people left the provinces for the capital with the hope that they would have access to employment and better living conditions.

Figure 17a,b shows a series of socioeconomic factors, including population density, transport infrastructure, and annual income, interconnected with a range of geotechnical hazards, including landslides, liquefaction potential, and the spatial distribution of earthquake intensity corresponding to the 2021 seismic event. The highest population density, the lowest income level, the highest risk of soil liquefaction, and the highest earthquake intensity overlap in the southern region of Haiti, compromising the most vulnerable urban areas (e.g., Les Cayes). The locations of our study sites for liquefaction assessment (i.e., BLC1-BLC5; see Fig. 15) fall within the darker area in Figure 17b (mostly in Les Cayes), which represents a higher probability of liquefaction. Not surprisingly, the south western portion of Les Cayes has younger, uncemented, Quaternary surficial deposits and low proxy-based V_{S30} values (see Figs. 6 and 8).

The city of Les Cayes has been identified as the area most notably affected by the 2021 event (Dashti *et al.*, 2022) and has also been affected by the previous natural disasters, while simultaneously experiencing a population inflow since 2010 (Fig. 16). Figure 17 can help explain how the impact on those communities was exacerbated as a result of the area been significantly impacted by landslides (dark gray crosses in Fig. 17b), which affected several of the main transportation routes (particularly RN7 in Fig. 17a). The USGS rated the

landslide risk as "orange" after the 2021 event to indicate a significant area affected and significant population exposed. Intersectional maps show that the areas impacted by the 2021 earthquake are vulnerable to a range of geotechnical hazards that will impact immediate and long-term recovery from the 2021 earthquake and are likely to make communities vulnerable to future hazards including earthquakes, landslides, and hurricanes. People mobilization patterns (in response to specific socioeconomic and political boundary conditions, such as extreme poverty and the presence of NGOs) and the formation of IDP camps, very often without guidance of the scientific community on the exposure to natural hazards at those locations, make intersectional maps a useful tool for more appropriate assessments of the intersections of engineering and social science aspects of disaster recovery and resilience practices.

Intersectional maps shown in Figures 16 and 17 were created using a simplified base map layer of the geographic extent of Haiti, which was downloaded from the digital cartography collection of Porto Tapiquén (2020). Subsequently, several maps that include different engineering data or social aspects were superimposed as multiple base map layers either manually or digitally. For instance, USGS liquefaction or landslides probability map images were overlaid on the main base map by manually assigning map coordinates to some points of the image. Other map features include objects, data points, and contours to better visualize the available data. For example, some base map layers include a group of georeferenced objects manually traced (e.g., polygons that represent Haiti communes) with different attributes (e.g., total population per commune). Maps also include layers with data points corresponding to the coordinates of the epicenters for both the 2021 Nippes earthquake and the 2010 Port-au-Prince earthquake. The intersectional map in Figure 16 provides a visual representation of qualitative and quantitative tabulated data (e.g., the disaster new population displacement arrows). When possible, available data were postprocessed for easier visual interpretation. For instance, earthquake intensity contours from USGS (2021) were digitalized to more easily overlay them on the main base map layer.

Lessons from a hybrid reconnaissance approach

The remote GEER team consisted of experts in geotechnical earthquake engineering, engineering geology and seismology, engineering geomorphology, and social and political implications of disasters. Because of the nature of this event and lack of immediate physical presence of the team (due to safety and security concerns), we initially collected perishable data and information from a variety of sources as quickly as possible. For example, the team employed reports provided by the USGS, USAID, CNIGS, CNSA, UN, and World Bank, satellite imagery, drone data collected by the World Bank. We obtained ground motion recordings from IRIS, Raspberry Shake Citizen Science Network Ayiti-Seismes of Haiti, and Observatorio Sismológico Politécnico Loyola (in Dominican Republic). Evidence of geotechnical damage in affected areas was initially collected from social media (primarily twitter) and mainstream media as well as satellite imagery (primarily Google Earth) during reconnaissance planning. Subsequently, field reconnaissance was conducted with local GEER team members in affected areas. Social science data mainly relied on our team's prior research in Haiti following the 2010 earthquake and a review of secondary sources. Examples of secondary sources include: (1) Haitian government agencies (e.g., Ministry of Public Health [Ministère de la Santé Publique et de la Population]); (2) Haitian (e.g., Quisqueya University [Université Quisqueya]) and international universities, think tanks, and research institutes (e.g., Pew Research Center); (3) Haitian (e.g., Le Nouvelliste) and international news sources (e.g., Reuters); (4) international aid agencies (e.g., the World Bank, the UNDP, UN Office for Coordination of Humanitarian Assistance, UN International Organization for Migration, and UN Security Council); and (5) disaster-focused databases (e.g., EM-DAT International Disaster Database).

Our goal in this study was to evaluate geotechnical and seismological hazards and consequences in conjunction with socioeconomic–political obstacles and crises, and evaluate their intersection (i.e., intersectional impacts) in Haiti, to guide future research or mitigation decisions. This led to the creation of intersectional maps that combine information on socioeconomic settings with ground shaking, liquefaction, or landslide probability as a few examples of seismological and geotechnical hazards. These maps helped identify the spatiotemporal overlap of severe hazards with severe economic conditions or population displacements that are alarming. The compounded nature of these crises and consequences can guide future research and mitigation planning. Further, an in-depth review of the timeline and intensity of socioeconomic–political crises in Haiti can guide a process of obtaining more comprehensive, practical, and equitable ground motion recordings in the future, as well as other seismological and geotechnical hazards and phenomena.

CONCLUSIONS AND FUTURE DIRECTIONS

This study builds upon the interdisciplinary GEER team efforts on the collection of perishable data and documentation of relevant case studies from the 2021 Nippes earthquake. The latter occurred in conjunction with significant social, economic, and political challenges as well as other hazards (e.g., storm and a global pandemic) that made the population especially vulnerable to the aftermath of this earthquake. As a result, a hybrid approach to postearthquake reconnaissance was undertaken, which included a remote team working in close collaboration with local colleagues and students from Haiti in the field. Our goal was to investigate the effects and consequences that are at the intersection of geotechnical earthquake engineering and social science (what we refer to as intersectional impacts).

Unlike the 2010 M_w 7.0 Port-au-Prince earthquake, recordings from the 2021 mainshock are available. A velocity pulse is observed in the fault-normal direction of a near-source ground motion, but further investigation is necessary to confirm directivity effects. Potential site effects are evaluated by investigating subsurface conditions in the region, and by conducting single station analyses at stations that recorded the mainshock and aftershocks. A new geology-informed V_{S30} map that implemented the geostatistical approach of kriging with external drift (which is a form of regression–kriging) while accounting for in situ measurements of V_{S30} is proposed for Les Cayes and Port-au-Prince. Reduced variability is obtained when comparing kriged V_{S30} values to topographic slope proxy-based and geology only-informed V_{S30}. However, more detailed, and high-quality subsurface characterization in Les Cayes and other affected regions after the 2021 event, such as Nippes and Jérémie, is necessary for validation efforts, and to improve our understanding of local site conditions and regional site amplification patterns. Single station analyses at the station located in the U.S. Embassy (i.e., AY.NQUSE) provided evidence of systematic contributions from sedimentary deposits to the observed ground motions. Increasing the availability, accessibility, and sustainability of ground-motion records in Haiti is essential to improve the characterization of seismic hazards in the region. Likewise, additional V_S profiling directed at high-impact areas would provide the necessary subsurface characterization to further understand potential site effects.

Lessons from geotechnical engineering case studies on landslides and liquefaction triggering are presented, and potential mechanisms of failure are explored. 2D slope rockfall analyses were performed to investigate the role of an existing gabion wall in the observed damage along RN7. Findings from these analyses showed that the presence of the gabion wall significantly hindered the trajectory of rock debris, which was consistent with the observations made by the GEER team. In addition, LPI values were computed to assess the extent of expected damage due to liquefaction triggering at specific locations where data were available. Values of LPI ranging from 24 to 32.5 indicated that major damage was expected at one of the study sites where field observations of possible lateral spreading near south Les Cayes were reported by the GEER team in situ.

Finally, we described the intersections between engineering observations and social sciences, focusing on the vulnerability of communities in Haiti to multiple natural hazards, and governance, security, developmental, and mental health challenges. In general, we found that the recent natural hazards and social conflicts have affected the population's vulnerability to earthquake-induced failure of infrastructure. More specifically, four areas of intersection are also identified: (1) response-oriented humanitarian involvement as opposed to long-term developmental focus; (2) increasing preparedness in the face of uncertain natural hazards is challenging, given Haiti's current and multifaceted crises; (3) emergent citizen science efforts; and (4) migration patterns driven by extreme poverty and NGOs. These intersections are further explored in the creation of intersectional maps and shaped by our hybrid (i.e., remote and in situ) and interdisciplinary reconnaissance approach.

Intersectional maps were developed to illustrate how the intersection of engineering aspects (e.g., seismic hazard spatial distribution, landslide inventory from the 2021 earthquake, and liquefaction potential) and social science (e.g., population movement, average annual income, and population density) provides a more complete and in-depth picture of the aftermath from the 2021 Nippes earthquake. The visualization of these important intersections can enable the next generation of human-centered approaches for disaster resilience research and practice.

DATA AND RESOURCES

The geologic map geodatabase used in the assessment of geology-based proxy V_{S30} (Figs. 2, 5, 6, and 8) was prepared using ArcGIS, and it is presented for use at a nominal scale of 1:500,000 by Wilson *et al.* (2019). The geologic map (scale 1:250,000) obtained from the Bureau des Mines et de l'Energie d'Haiti (Rathje *et al.*, 2010; last accessed September 2021) was consulted when possible. To obtain the geology-based proxy V_{S30} values, all in-situ V_{S30} measurements and standard penetration tests (SPT)-N values were collected from multichannel analysis of surface waves (MASW) 1D tests and SPT tests results reported in http://geotechmap.ueh.edu.ht/#/dashboard (last accessed June 2022), respectively. The shapefiles boundaries used for Haiti, Les Cayes, and Port-au-Prince within ArcGIS Pro to develop the maps in Figures 2, 6, and 8 were extracted from Centre National de l'Information Géo-Spatiale (CNIGS, last accessed February 2022). Seismograms used in this study were collected as part of the Ayiti Seismic Network available at https://ayiti.unice.fr/ayiti-seismes/ (last accessed June 2021) and Raspberry Shake. Data can be obtained from the SeisComp3 RaspberryShake (Raspberry Shake 2016) at http://www.fdsn.org/datacenters/detail/RASPISHAKE/ (last accessed May 2022) and Incorporated Research Institutions for Seismology (IRIS) Data Management Center at https://www.iris.edu (last accessed May 2022). The peak ground acceleration (PGA) shakemap was downloaded from U.S. Geological survey (USGS) (last accessed October 2021). The World Bank gross domestic product (GDP) per capita data were collected (https://data.worldbank.org/indicator/NY.GDP.PCAP.CD?end=2020&locations=CO-BO-HT-MX-EC-CU-PE-HN-GT-NI&most_recent_year_desc=false&start=2010&view=chart, last accessed December 2022) as part of the social science perspective of disasters. Data on humanitarian response were obtained from ReliefWeb (https://reliefweb.int/report/haiti/2021-haiti-earthquake-situation-report-10-december-16-2021, last accessed December 2022)—a humanitarian information service for the United Nations Office for the Coordination of Humanitarian Affairs. International remittance flow data were obtained from the Pew Research Center (https://www.pewresearch.org/global/interactives/remittance-flows-by-country/, last accessed December 2022). COVID-19 data were obtained from the Haitian Ministry of Health (Ministère de Santé Publique et de la Population, http://www.mspp.gouv.ht/documentation/?txt_date_debut=&start=0&txt_date_fin=&txt_categorie

=10&txt_mot_cle=&btn_search=, last accessed December 2022). Data on disasters in Haiti were obtained from the International Disaster Database (EM-DAT, https://public.emdat.be, last accessed December 2022). Changes in population density were obtained from MapAction (https://mapaction.org, last accessed December 2022). The displacements linked to disasters in Haiti are available in Internal Displacement Monitoring Centre (IDMC) in https://data.humdata.org/dataset/idmc-idp-data-for-haiti (last accessed September 2021). And the information comes from Bureau des mines et de l'Énergie d'Haïti in http://www.bme.gouv.ht/carte/index.html (last accessed September 2021). Satellite imagery shows that significant landslide activity in the mountainous terrain of Pic Macaya National Park primarily from the August 16 arrival of Tropical Storm Grace is in https://earthobservatory.nasa.gov/images/148713/earthquake-in-haiti-triggers-landslides and planet.com (last accessed December 2022) provided by Adam Voiland of National Aeronautics and Space Administration (NASA) Earth Observatory and Planet Labs, respectively (last accessed September 2021). The software RocFall2 is in https://www.rocscience.com/software/rocfall (last accessed September 2021). The SPT boreholes (BLC1-BLC5) are provided by State University of Haiti in http://geotechmap.ueh.edu.ht/#/dashboard (last accessed October 2021). The crime data are provided by Insight crime in https://insightcrime.org/news/insight-crimes-2021-homicide-round-up/ and https://insightcrime.org/wp-content/uploads/2022/01/2022-01-17-Haiti-Homicides-2021.jpg (last accessed February 2022). The data reported by U.S. Agency for International Development (USAID) are in https://reliefweb.int/report/haiti/haiti-earthquake-fact-sheet-39-fiscal-year-fy-2010 (last accessed December 2022) (i.e., Fact Sheet number 39, Fiscal Year 2010) and in https://pdf.usaid.gov/pdf_docs/PA00J3GP.pdf (last accessed December 2022) (i.e., Fact Sheet number 4, Fiscal Year 2011). Pdfs (i.e., map of earthquake-affected areas and population movement in Haiti) were last accessed in September 2021. The cited cable news network news "Surging gang violence in Haiti's capital leaves nearly 200 dead in one month" is in https://www.cnn.com/2022/05/31/americas/haiti-gang-violence-intl/index.html (last accessed June 2021). The other relevant data to this article are available at USGS (https://www.usgs.gov/, last accessed September 2021).

DECLARATION OF COMPETING INTERESTS

The authors acknowledge that there are no conflicts of interest recorded.

ACKNOWLEDGMENTS

The authors would like to acknowledge the support of the U.S. National Science Foundation (NSF) through GEER. In addition, this research was partially funded by NSF grant Number CMMI-2145466. This support is gratefully acknowledged. Any opinions or findings presented in this report are those of the authors and do not necessarily reflect the viewpoint of the NSF. The authors would also like to express their gratitude to the U.S Geological Survey (USGS) for providing access to hazard maps. In addition, the team benefited greatly from collaboration and coordination with members of Structural Extreme Events Reconnaissance (StEER) and GeoHazards International (GHI), who were collecting data on both structural and geotechnical hazards in Haiti immediately following the 2021 earthquake. StEER also provided access to the phone application Fulcrum, which greatly improved our ability to collect relevant perishable data on the ground. Finally, the authors would like to thank two anonymous reviewers whose suggestions helped improved the quality of this article.

REFERENCES

Bent, A. L., J. Cassidy, C. Prépetit, M. Lamontagne, and S. Ulysse (2018). Real-time seismic monitoring in Haiti and some applications, *Seismol. Res. Lett.* **89,** no. 2A, 407–415, doi: 10.1785/0220170176.

Blanc, J., G. J. Rahill, S. Laconi, and Y. Mouchenik (2016). Religious beliefs, PTSD, depression and resilience in survivors of the 2010 Haiti earthquake, *J. Affect Disord.* **190,** 697–703, doi: 10.1016/j.jad.2015.10.046.

Boulanger, R. W., and I. M. Idriss (2014). *CPT and SPT Based Liquefaction Triggering Procedures, UCD/CGM-14/01*, Center for Geotechnical Modeling, Department of Civil and Environmental Engineering, University of California, Davis, California.

Bradley, M. (2012). Notes from the field: Haiti-displacement and development in the Republic of NGOs (last accessed September 2014).

Brière, S., S. Jobert, and Y. Poulin (2010). Enhancing public governance in fragile states: Support for Haiti, *Int. J.* **65,** no. 3, 653–667.

Butterlin, J. (1960). *Géologie générale et régionale de la république d'Haïti*, Éditions de l'IHEAL, Paris (in French).

Cabas, A., C. Ji, N. Ingabire Abayo, C. Lorenzo-Velazquez, R. Lagesse, K. Guerrier, N. Saint Fleur, S. Dashti, F. E. Garcia, J. Ramirez, *et al.* (2022). Seismological aspects and ground motion characteristics from the 2021 M 7.2 Nippes Haiti earthquake, *12th National Conf. of Earthquake Engineering*, Salt Lake City, Utah.

Calais, E., D. Boisson, S. Symithe, R. Momplaisir, C. Prépetit, S. Ulysse, G.P. Etienne, F. Courboulex, A. Deschamps, T. Monfret, *et al.* (2019). Monitoring Haiti's quakes with raspberry shake, *Eos Trans. AGU* 100.

Calais, E., D. Boisson, S. Symithe, C. Prépetit, B. Pierre, S. Ulyse, L. Hurbon, A. Gilles, J. M. Théodat, T. Monfret, *et al.* (2020). A socio-seismology experiment in Haiti, *Front. Earth Sci.* **8,** 542,654, doi: 10.3389/feart.2020.542654.

Calais, E., S. Symithe, T. Monfret, B. Delouis, A. Lomax, F. Courboulex, J. P. Ampuero, P. E. Lara, Q. Bletery, J. Chèze, *et al.* (2022). Citizen seismology helps decipher the 2021 Haiti earthquake, *Science* **376,** no. 6590, 283–287, doi: 10.1126/science.abn1045.

CDC and Interuniversity Institute for Research and Development (INURED) (2014). *Violence Against Children in Haiti: Findings from a National Survey, 2012*, Centers for Disease Control and Prevention, Port-au-Prince, Haiti.

Collier, P. (2008). *The Bottom Billion: Why the Poorest Countries are Failing and What Can Be Done About It*, Oxford University Press, U.S.A.

Contreras, S. (2019). Using Arnstein's Ladder as an evaluative framework for the assessment of participatory work in Postdisaster Haiti, *J. Am. Plann. Assoc.* **85,** no. 3, 219–235, doi: 10.1080/01944363.2019.1618728.

Cox, B. R., J. Bachhuber, E. Rathje, C. M. Wood, R. Dulberg, A. Kottke, R. A. Green, and S. M. Olson (2011). Shear wave velocity- and geology-based seismic microzonation of Port-au-Prince, Haiti, *Earthq. Spectra* **27,** 67–92, doi: 10.1193/1.3630226.

Cox, B. R., T. Cheng, J. P. Vantassel, and L. Manuel (2020). A statistical representation and frequency-domain window-rejection algorithm for single-station HVSR measurements, *Geophys. J. Int.* **221,** no. 3, 2170–2183, doi: 10.1093/gji/ggaa119.

Dashti, S., N. E. Ganapati, N. Ingabire Abayo, A. Cabas, J. Ramirez, S. Contreras, J. E. Dessable, F. E. Garcia, K. Guerrier, Y. Hwang, *et al.* (2022). Reconnaissance following the August 14, 2021 Haiti earthquake: Perspective from geotechnical engineering and social/political sciences, *GEER (Report-73)*.

Dawood, H. M., A. Rodriguez-Marek, J. Bayless, C. Goulet, and E. Thompson (2016). A Flatfile for the KiK-net database processed using an automated protocol, *Earthq. Spectra* **32,** no. 2, 1281–1302, doi: 10.1193/071214eqs106.

Desvarieux, J., and N. Harris (2010). *Haiti earthquake: Pictures of Port-au-Prince Tent Cities|Time*, available at https://time.com/3774903/richard-mosse-the-tent-cities-of-haiti (last accessed 22 September 2022).

Eberhard, M., S. Baldridge, J. Marshall, W. Mooney, and G. Rix (2010). *The MW 7.0 Haiti earthquake of January 12, 2010, USGS/EERI Advance Reconnaissance Team Rept., U.S. Geol. Surv. Open-File Rept. 2010-1048*, 64 pp.

Elliott, J., and L. Sullivan (2015). How the red cross raised half a Billion Dollars for Haiti and Built Six Homes, Pro Publica.

EM-DAT (2021). The international disasters database, available at https://www.emdat.be/ (last accessed 23 September 2021).

Fanm, K. (2012). Appel à la mobilisation citoyenne et à la solidarité en faveur de la construction Nationale (Call for citizen mobilization and solidarity in favor of national construction), Port-au-Prince, Haiti, 1639 (in French).

Fanning, S. C. (2007). The roots of early black nationalism: northern African Americans' invocations of Haiti in the early nineteenth century, *Slavery Abolit.* **28,** no. 1, 61–85, doi: 10.1080/01440390701269780.

Fatton, R. (2002). *Haiti's Predatory Republic: The Unending Transition to Democracy*, Lynne Rienner Publishers, Boulder, Colorado.

Fischer, A., and M. Levy (2012). Designing environmental restoration programs in politically fragile states: Lessons from Haiti, doi: 10.13140/RG.2.1.2685.3607.

Foster, K. M., B. A. Bradley, C. R. McGann, and L. M. Wotherspoon (2019) A VS30 map for New Zealand based on geologic and terrain proxy variables and field measurements, *Earthq. Spectra* **35,** no. 4, 1865–1897

French, C. D., and C. J. Schenk (2004). *Surface geology of the Caribbean region (geo6bg)*, U.S. Geological Survey data release, doi: 10.5066/P938YEBH

Ganapati, N. E., and A. Mukherji (2019). "House keeping": Managing post-disaster housing recovery long term, Housing Recovery after Disasters, 167.

Ganapati, N. E., and G. J. Rahill (2017). *Early Post-Disaster Shelter Recovery in Fragile States: A Case of the 12 January 2010 Haiti Earthquake*, CRC Press, Taylor and Francis Group, Boca Raton, Florida.

Garcia, F. E., J. Ramirez, A. Cabas, C. Ji, N. Ingabire Abayo, C. Lorenzo-Velazquez, R. Lagesse, K. Guerrier, N. Saint Fleur, S. Dashti, *et al.* (2022). Geotechnical aspects of the 2021 Mw 7.2 Nippes, Haiti earthquake, *12th National Conf. of Earthquake Engineering*, Salt Lake City, Utah, 27 June–1 July 2022.

Gelting, R., K. Bliss, M. Patrick, G. Lockhart, and T. Handzel (2013). Water, sanitation and hygiene in Haiti: Past, present, and future, *Am. J. Trop. Med. Hyg.* **89,** no. 4, 665–670, doi: 10.4269/ajtmh.13-0217.

Goovaerts, P. (1997). *Geostatistics for Natural Resources Evaluation*, Oxford University Press on Demand, New York, New York.

Hallward, P. (2007). *Damming the Flood: Haiti, Aristide, and the Politics of Containment*, Verso, London, New York.

Hearne, M., E. M. Thompson, H. Schovanec, J. Rekoske, B. T. Aagaard, and C. B. Worden (2019). USGS automated ground motion processing software, *U.S. Geol. Surv* doi: 10.5066/P9ANQXN3.

Human Rights Watch (2020). Haiti: Events of 2020, *World Rept. 2021*.

Internal Displacement Monitoring Centre (IDMC) (2020). *Behind the numbers: The shadow of 2010's earthquake still looms large in Haiti*, available at https://www.internal-displacement.org/expert-opinion/behind-the-numbers-the-shadow-of-2010s-earthquake-still-looms-large-in-haiti (last accessed 12 October 2022).

Internal Displacement Monitoring Centre (2021). *Haiti—Internally displaced persons—IDPs—Humanitarian Data Exchange*, available at https://data.humdata.org/dataset/idmc-idp-data-for-haiti (last accessed 29 September 2021).

International Organization for Migration (2022). *Haïti – Système d'Alerte Précoce Pour Les Déplacements—Zone Métropolitaine De Port-au-Prince (23 Avril–06 Mai 2022)*, available at https://displacement.iom.int/reports/haiti-systeme-dalerte-precoce-pour-les-deplacements-zone-metropolitaine-de-port-au-prince?close=true (last accessed 19 June 2022) (in French).

Iwasaki, T. (1978). A practical method for assessing soil liquefaction potential based on case studies at various sites in Japan, *Proc. of the Second Int. Conf. Microzonation Safer Construction Research Application*, 885–896.

Jones, J. N., M. Stokes, S. J. Boulton, G. L. Bennett, and M. R. Z. Whitworth (2020). Coseismic and monsoon-triggered landslide impacts on remote trekking infrastructure, Langtang Valley, Nepal, *Q. J. Eng. Geol. Hydrogeol.* **53,** no. 2, 159–166.

Joshi, M., G. J. Rahill, and S. Rhode (2021). Comparison of trauma symptoms among nonpartner sexual violence victims and nonvictims in Urban Haiti's Cité Soleil neighborhood, *J. Black Psychol.* **47,** nos. 4/5, 284–316, doi: 10.1177/0095798421997217.

Konno, K., and T. Ohmachi (1998). Ground-motion characteristics estimated from spectral ratio between horizontal and vertical components of microtremor, *Bull. Seismol. Soc. Am.* **88,** no. 1, 228–241, doi: 10.1785/BSSA0880010228.

Kristoff, M., and L. Panarelli (2010). Haiti: A republic of NGOs?, in *Peace brief*, United States Institute of Peace, Washington, D.C.

Kroll, A., C. L. Remington, P. Awasthi, and N. E. Ganapati (2021). Mitigating the negative effects of emotional labor: A study of disaster response and recovery workers after the 2010 Haiti earthquake, *Governance* **34,** no. 1, 87–106, doi: 10.1111/gove.12476.

Kwok, T. C. (2016). *Continued challenges in rebuilding Haiti*, available at https://www.e-ir.info/2016/03/11/continued-challenges-in-rebuilding-haiti (last accessed 24 September 2021).

Le Nouvelliste (2021). Covid-19: Les variants Delta et MU présents en Haïti, selon le Ministère de la Santé Publique et de la Population, available at https://lenouvelliste.com/alaminute/19727/covid-19-les-variants-delta-et-mu-presents-en-haiti-selon-le-mspp (last accessed December 2022) (in French).

Li, M., E. M. Rathje, B. R. Cox, and M. Yust (2022). A Texas-specific VS30 map incorporating geology and VS30 observations, *Earthq. Spectra* **38,** no. 1, 521–542, doi: 10.1177/87552930211033622.

Marcelin, L. H., and T. Cela (2020). Justice and rule of law failure in Haiti: A view from the Shanties, *J. Commun. Psychol.* **48,** no. 2, 267–282, doi: 10.1002/jcop.22249.

Marcelin, L. H., T. Cela, and J. M. Shultz (2016). Haiti and the politics of governance and community responses to Hurricane Matthew, *Disaster Health* **3,** no. 4, 151–161, doi: 10.1080/21665044.2016.1263539.

Martinez, S. N., K. E. Allstadt, S. L. Slaughter, R. G. Schmitt, E. Collins, L. N. Schaefer, and S. Ellison (2021). *Rapid response landslide inventory for the 14 August 2021 M7.2 Nippes, Haiti, U.S. Geol. Surv. Open-File Rept. No. 2021-1112*.

McKey, C. (2016). *The Economic Consequences of the Haitian Revolution*, University of Oregon, Eugene, Oregon.

Mérancourt, W., and A. Faiola (2021). Abductions by the busload: Haitians are being held hostage by a surge in kidnappings, *The Washington Post*, available at https://www.washingtonpost.com/world/2021/10/09/haiti-kidnapping/ (last accessed December 2022).

Nakamura, Y. (1989). A method for dynamic characteristics estimation of subsurface using microtremor on the ground surface, *Railway Technical Research Institute, Quarterly Reports*, 30**,** no. 1, 25–33.

Parker, G. A., J. A. Harmon, J. P. Stewart, Y. M. A. Hashash, A. R. Kottke, E. M. Rathje, W. J. Silva, and K. W. Campbell (2017). Proxy-based V_{S30} estimation in central and eastern North America, *Bull. Seismol. Soc. Am.* 107**,** no. 1, 117–131, doi: 10.1785/0120160101.

Pérodin, J., Z. Adefris, M. Cruz, N. Matos Rondon, L. Hermantin, G. De la Cruz, N. E. Ganapati, and S. Ganapati (2021). Reconceptualizing disaster phases through a Metis-based approach, *Disaster Prev. Manag.* **31,** no. 3, 288–303, doi: 10.1108/DPM-02-2021-0060.

Porto Tapiquén, C. E. (2020). *Orogénesis Soluciones Geográficas*, Porlamar, Venezuela 2015, Based on shapes from Enviromental Systems Research Institute (ESRI).

Pritchett, L., M. Woolcock, and M. Andrews (2013). Looking like a state: Techniques of persistent failure in state capability for implementation, *J. Dev. Stud.* **49,** no. 1, 1–18, doi: 10.1080/00220388.2012.709614.

Rahill, G. J., M. Joshi, J. Galea, and J. Ollis (2020). Experiences of sexual and gender minorities in an urban enclave of Haiti: Despised, beaten, stoned, stabbed, shot and raped, *Cult. Health Sex.* **22,** no. 6, 690–704, doi: 10.1080/13691058.2019.1628305.

Rahill, G. J., M. Joshi, C. Lescano, and D. Holbert (2015). Symptoms of PTSD in a sample of female victims of sexual violence in post-earthquake Haiti, *J. Affect. Disord.* **173,** 232–238, doi: 10.1016/j.jad.2014.10.067.

Ramachandran, V., and J. Walz (2015). Haiti: Where has all the money gone? *J. Haitian Stud.* **21,** no. 1, 26–65.

Ramos-Sepúlveda, M. E., and A. Cabas (2021). Site effects on ground motion directionality: Lessons from case studies in Japan, *Soil Dyn. Earthq. Eng.* **147,** 106755, doi: 10.1016/j.soildyn.2021.106755.

Ramos-Sepúlveda, M. E., G. A. Parker, E. M. Thompson, S. J. Brandenberg, M. Li, O. Ihann, Y. M. A. Hashash, E. M. Rathje, and J. P. Stewart (2022). High-pass corner frequency selection for implementation in the USGS automated ground motion processing tool, *Seismol. Res. Lett.* **93,** no. **2B**, 1115–1372, doi: 10.1785/0220220087.

Rathje, E., J. Bachhuber, B. Cox, J. French, R. Green, S. Olson, G. Rix, and D. Wells (2010). *Geotechnical engineering reconnaissance of the 2010 Haiti earthquake*, *GEER*, 97 pp.

ReliefWeb (2021). *Deadly surge in gang violence in Haiti's capital displaces nearly twice as many people in June than in all of 2020—Haiti|ReliefWeb*, available at https://reliefweb.int/report/haiti/deadly-surge-gang-violence-haiti-s-capital-displaces-nearly-twice-many-people-june-all (last accessed 12 October 2022).

Remington, C. L., and N. E. Ganapati (2017). Recovery worker skills in post-earthquake Haiti: The disconnect between employer and employee perspectives, *Nat. Hazards* **87,** no. 3, 1673–1690, doi: 10.1007/s11069-017-2840-4.

Rocscience (2021). Rocfall 2D software, Rocscience Inc.

Schuller, M., 2017, Haiti's Republic of NGOs, *Curr. Hist.* **116,** no. 787, 68–73.

Shultz, J. M., T. Cela, L. H. Marcelin, M. Espinola, I. Heitmann, C. Sanchez, A. Jean Pierre, C. Y. Foo, K. Thompson, P. Klotzbach, *et al.* (2016). The trauma signature of 2016 Hurricane Matthew and the psychosocial impact on Haiti, *Disaster Health* **3,** no. 4, 121–138, doi: 10.1080/21665044.2016.1263538.

Sontag, D. (2012). *Years After Haiti Quake, Safe Housing is a Dream for Many*, The New York Times, New York City, New York.

Styron, R. H., J. García-Pelaez, and M. Pagani (2018). *GEM Central America and Caribbean Active Faults Database*, available at https://doi.org/10.13117/CENTRAL-AMERICA-CARIBBEAN-ACTIVE-FAULTS (last accessed December 2022).

Thompson, E. M., D. J. Wald, and C. B. Worden (2014). A VS30 map for California with geologic and topographic constraints, *Bull. Seismol. Soc. Am.* **104,** no. 5, 2313–2321, doi: 10.1785/0120130312.

UN International Strategy for Disaster Reduction (UNISDR) (2013). *Department of Economic and Social Affairs*, available at https://sdgs.un.org/ar/node/8377 (last accessed 15 October 2021).

UNDP (2009). *Human Development Report 2009*, United Nations Development Programme, New York.

UNDP (2015). *Human Development Reports: Human Development Index (HDI)*, United Nations Development Programme, New York.

UNDP (2020). *Human Development Report: The Next Frontier: Human Development and the Anthropocene*, United Nations Development Programme, New York.

USGS (2021). *Pager Alert Version 8*, available at https://earthquake.usgs.gov/earthquakes/eventpage/us6000f65h/executive (last accessed December 2022).

Wald, D. J., and T. I. Allen (2007). Topographic slope as a proxy for seismic site conditions and amplification, *Bull. Seismol. Soc. Am.* **97,** no. 5, 1379–1395, doi: 10.1785/0120060267.

Wang, P., P. Zimmaro, T. E. Buckreis, T. Gospe, S. J. Brandenberg, S. K. Ahdi, A. Yong, and J. P. Stewart (2022). Relational database for horizontal-to-vertical spectral ratios, *Seismol. Res. Lett.* **93,** no. 2A, 1075–1088, doi: 10.1785/0220210128.

Whitworth, M. R. Z., S. J. Boulton, and J. N. Jones (2020b). Implementing the Sendai Framework in developing countries using remote sensing techniques for the evaluation of natural hazards, *Lowl. Technol. Int.* **22,** no. 1, 113–122.

Whitworth, M. R. Z., G. Giardina, C. Penney, L. Di Sarno, K. Adams, T. Kijewski-Correa, J. Black, F. Foroughnia, V. Macchiarulo, P. Milillo, *et al.* (2022). Lessons for remote post-earthquake reconnaissance from the 14 August 2021 Haiti earthquake, *Front. Built Environ.* 53, doi: 10.3389/fbuil.2022.873212.

Whitworth, M. R. Z., A. Moore, M. Francis, S. Hubbard, and S. Manandhar (2020a). Building a more resilient Nepal-the utilisation of the resilience scorecard for Kathmandu, Nepal following the Gorkha earthquake of 2015, *Lowl. Technol. Int.* **21,** no. 4, 229–236.

Willman, A., and L. H. Marcelin (2010). If they could make us disappear, they would! Youth and violence in Cité Soleil, Haiti, *J. Community Psychol.* **38,** no. 4, 515–531, doi: 10.1002/jcop.20379.

Wills, C. J., and K. B. Clahan (2006). Developing a map of geologically defined site-condition categories for California, *Bull. Seismol. Soc. Am.* **96,** no. 4A, 1483–1501, doi: 10.1785/0120050179.

Wilson, F. H., G. Orris, and F. Gray (2019). Preliminary geologic map of the greater Antilles and the Virgin Islands, *Open-File Rept. 2019-1036*.

World Bank (2011). *World Development Report 2011: Conflict, Security, and Development*, World Bank, Washington, D.C.

World Bank (2019). Rebuilding Haitian Infrastructure and Institutions available at https://www.worldbank.org/en/results/2019/05/03/rebuilding-haitian-infrastructure-and-institutions (last accessed 23 October 2021).

World Bank (2021). Haiti overview, available at https://data.worldbank.org/indicator/NY.GDP.PCAP.CD?end=2020&locations=CO-BO-HT-MX-EC-CU-PE-HN-GT-NI&most_recent_year_desc=false&start=2010&view=chart (last accessed 12 September 2021).

World Population Review (2021). Haiti population, available at https://worldpopulationreview.com/countries/haiti-population (last accessed 12 September 2021).

Zalachoris, G., E. M. Rathje, and J. G. Paine (2017). V_{S30} characterization of Texas, Oklahoma, and Kansas using the P-wave seismogram method, *Earthq. Spectra* **33,** no. 3, 943–961, doi: 10.1193/102416eqs179m.

Zanotti, L. (2010). Cacophonies of aid, failed state building and NGO s in Haiti: Setting the stage for disaster, envisioning the future, *Third World Q.* **31,** no. 5, 755–771, doi: 10.1080/01436597.2010.503567.

Zhu, C., M. Pilz, and F. Cotton (2020). Evaluation of a novel application of earthquake HVSR in site-specific amplification estimation, *Soil Dynam. Earthq. Eng.* **139,** 106301, doi: 10.1016/j.soildyn.2020.106301.

Manuscript received 21 June 2022
Published online 4 January 2023